PERGAMON

International Journal of Multiphase Flow 28 (2002) 823–863

International Journal of Multiphase Flow

www.elsevier.com/locate/ijmulflow

On the modelling of multiphase turbulent flows for environmental and hydrodynamic applications

Djamel Lakehal

Institute of Energy Technology, ETH Zurich, ETH-Zentrum/CLT2, CH-8092 Zurich, Switzerland

Received 1 November 2000; received in revised form 24 November 2001

Abstract

The paper examines a selection of well-established prediction methods employed for the modelling of multiphase turbulent flows presented in typical environmental and hydrodynamic applications. The main objective is to provide a basic understanding of the subject with a deliberate intention to simplifying the presentation. Turbulence is approached on the basis of the conventional one-point closure context. The experience gathered by the author and by others with various predictive strategies all based on the Eulerian–Eulerian (field description) and the Eulerian–Lagrangian methods are discussed and summarized; the goals, limitations, and required developments are described. Typical applications of each calculation method are presented, in which the interaction between the transported dispersed-phase and the field turbulence is treated on the basis of both one-way and two-way coupling. The case studies in question include aerosol production and transport over the oceans, pollutant dispersion in the atmospheric surface layer, hydrometeor impact on urban canopies, sedimentation of active sludge in secondary water clarifiers, and mixing and circulation within confined bubble plumes. Analysis of the various models reveals that for most of the reported applications the Reynolds averaged Navier–Stokes approach is inherently ill-posed and should be transcended by the promising large-eddy simulation concept.

Keywords: Turbulent-Flow; Droplets; Dilute Suspensions; Bubbles; Particles

1. Introduction

This paper is written in the spirit of an overview of different multiphase modelling methods, with emphasis on the practical motivations for certain selected applications and the expected

E-mail address: lakehal@iet.mavt.ethz.ch (D. Lakehal).

0301-9322/02/$ - see front matter
PII: S0301-9322(01)00086-6

returns from computational analyses. The role of simulation strategies in the prediction and design processes is also discussed. The deliberate choice of applications is motivated by the variety of solution methods applied in each case; we aim at discussing them in the sections to follow. The methods are discussed in a comprehensive and simplistic way based on known ideas and principles. An overview of the state-of-the-art is presented in treating the various subjects using the Eulerian–Eulerian method in both the one-fluid and two-fluid (interpenetrating media) formulations, as well as by the Eulerian–Lagrangian variant. Since the flows considered herein are presently out of reach of direct and large-eddy simulation approaches (DNS and LES), we essentially focus on the implications of turbulence modelling (by reference to the Reynolds Averaged Navier–Stokes Equations, RANS) in the various computational frameworks discussed in this paper, and the way this conventional approach could be improved on by more elaborate ones. In support of this, practical case studies typical of environmental and hydrodynamic applications are presented. Apart from the applications with reference to hydrodynamic applications CS5 and CS6, the interaction between the transported phase and the field turbulence is treated in all other cases on the basis of one-way coupling. Note, too, that the paper does not deal with simplified simulation approaches, for example, with the so-called *Gaussian models* employed for atmospheric dispersion modelling (cf. Hangan, 1999).

Eulerian–Eulerian and Eulerian–Lagrangian methods have been extensively used to simulate particle dispersion. Depending on the nature of the case studies in question it is possible to employ a specific form of each of the two solution methods. But prior to that, it is worth highlighting the main differences between these two strategies, i.e. the Eulerian–Eulerian vs. the Eulerian–Lagrangian methods. The choice between these two procedures is in essence problem-dependent. The Eulerian or field description methodology is commonly adopted for the prediction of interpenetrating media situations, including both highly particle loaded systems such as fluidized beds, dilute particle-laden flows as in the case of dilute suspensions of aerosols, droplets and particles, and gas–liquid mixtures such as bubbly flows. This approach can be employed in two distinctive forms: The one-fluid formulation and the two-fluid approach. In the first approach, generally employed in the form of a one-field description of highly-loaded or dilute suspensions formed by concentrations of droplets and particles, the particle concentrations are assumed to have some characteristics of a continuous phase (e.g. the local concentration) and, when appropriate, some of a dispersed phase (e.g. the inertial slip). In other words, the method essentially consists in solving an extra conservation law for the concentration of particles or for their mean spatial density. Modifications of the transport equations are also needed to consider buoyancy forces whenever the two phases exhibit differences in density due to the presence of a heavier dispersed phase (e.g. sedimentation problems, snow avalanches, etc.), or when the carrier phase features thermal stratification as is often the case in geophysical flows (e.g. thermal fronts, atmospheric surface layer, etc.). In addition, the transport equations must include interfacial exchange laws to account for mass transfer whenever the dispersed phase evaporates or condenses, e.g. evaporative marine droplets over the ocean. The combination of all these processes leads to a system of equations with a multitude of closure laws. In this respect, the closure relationships for the turbulent concentration or heat flux arising from Reynolds averaging conceptually follow the manner in which the mechanical turbulent stresses are approximated. This important issue is examined herein, too, in particular when the closure law for turbulence is a two-equation based approach, in which the buoyancy-induced contributions are represented in terms of additional

source terms in the turbulence equations with some adjustable coefficients. In the second approach, also known as the *six equation* model approach, the phases are treated as two interpenetrating continua evolving within a single system: Each point in the mixture is occupied simultaneously (in variable proportions) by both phases. Each phase is then governed by its own conservation and constitutive equations; these are then coupled through interphase interaction properties. More precisely, in contrast to the one-fluid formulation, convective and diffusive processes are explicitly taken into account in each of the two phases. For example, mixtures of two immiscible fluids such as air bubbles in water cannot be considered as mixtures of dilute suspensions evolving within a liquid phase; they have to be simulated via the two-fluid approach.

In the Lagrangian reference frame individual particles or clouds of particles are treated in a discrete way. The reference frame moves with the particles, and the instantaneous location of each particle is determined by reference to its origin and the time elapsed. Lagrangian methods employed for particle tracking are conventionally based on the equation of motion for spherical particles at high-Reynolds numbers, as given by Clift et al. (1978), also known as Basset–Boussinesq–Oseen (BBO) equation (cf. Crowe et al., 1996). The dispersed phases are assumed to be heavy and smaller than the Kolmogorov microscales. As a prerequisite computational sequence the flow field has to be known since tracking individual particles directly relies on its properties, i.e. velocity field and turbulence statistics. In practical applications the flow field is modelled by use of RANS, whereas the resort to DNS (Squires and Eaton, 1990; Mosyak and Hetsroni, 1999; Ahmed and Elghobashi, 2000; Sawford and Yeung, 2001) or LES (Yeh and Lei, 1991; Wang and Squires, 1996; Armenio et al., 1999; Boivin et al., 2000; Okong'o and Bellan, 2000) is still confined to research studies dealing for example with turbulence–particle interactions.

A variety of models accounting for the effects of turbulence on particle motion are available in the literature. A critical review of the variants employed for heavy particles in atmospheric turbulence is proposed by Wilson (2000). Another interesting review is that of Shirolkar et al. (1996) focusing on models used for dispersion in combustion problems. On the upper level of classification the models differ depending on whether they are applied to passive tracers (see, for example, Thomson, 1987) or to inertial particles (IP). The present work places emphasis on the second class of models only. A subcategory of IP dispersion models is an approach based on a Markov chain process, which is a finite discrete form of the Langevin equation supposed to model the fluctuating particle velocities in a purely stochastic way. This equation was first employed for the study of Brownian motion by Wang and Uhlenbeck (1945), and was only later applied to describe dispersion in homogeneous turbulence by Lin and Reid (1962). The other often employed random-flight algorithms treated in this paper are based on the generation of non-miscible (uncorrelated) random eddies, in which particle trajectories are purely deterministic. These are known as *eddy interaction models* (EIM), perhaps initially proposed by Gossman and Ioannides (1981). Here it is assumed that individual particles are subject to a series of interactions with randomly sampled eddies; the particle velocity remains constant during each particle–eddy interaction time, during which the eddy velocity remains unchanged. The difference between the two methods is that Markov chain type models provide a continuous fluctuating velocity field, whereas in EIMs the fluctuating velocity changes only when individual particles encounter a new eddy. This is the reason why MacInnes and Bracco (1992) refer to the first class as *continuous random walk models* and to the second as *discontinuous random walk models*.

The Eulerian–Lagrangian formalism thus amounts to the combination of two separate approaches: The Eulerian part delivers the flow field with its turbulent statistical properties, and the Lagrangian module employs these data to track individual particles. The parametrization of particle dispersion is therefore intimately tied to the dynamics of field turbulence. This is, of course, the case for dispersed phases smaller than the Kolmogorov micro-scales, whose interaction with turbulence is commonly termed *one-way coupling* by reference to the weak effect of particle momentum on turbulence. These two methods are here discussed in their original modelling context and in the LES framework.

Still, the Eulerian approach for simulating turbulent dispersion has its own advantages as compared to Lagrangian methods. For flow laden with a large amount of particles the quantitative description of the variation in particle concentration is much simpler by means of the Eulerian method since, for the same purpose, statistical sampling is required with the Lagrangian description. Lagrangian methods may also face problems whenever the cloud of particles tracked is larger than the fluid parcel over which volume averaging is performed. And apart from that, the Eulerian approach allows both phases to be computed over a single grid, whereas the Lagrangian methods require the interpolation of quantities between the fixed grid nodes and the local position of particles. However, treating particles via the Lagrangian formalism is in essence natural because their motion is tracked as they move through the flow field, which preserves their actual non-continuum behaviour and accounts for their history effects in a natural way. In addition, if attention is now redirected towards turbulence modelling, the Lagrangian approach holds a fundamental advantage over the Eulerian one in the sense that it does not require closure assumptions for turbulence correlations of tracer concentration and velocity fluctuations. More about the relative merits of these approaches is given by Durst et al. (1994) and Mostafa and Mongia (1987).

The present paper is structured as follows: Selected applications are first introduced to gradually highlight the expected results of computational analyses. These selected case studies (see Section 2) are referred to as CS1, CS2,...,CS6, respectively. Based on an extended literature survey the solution procedures employed so far in each case are introduced in Section 3. Section 4 is devoted to computational examples, where the solution methods are examined in the light of calculation results. Finally, key remarks are made in connection with computational strategies and turbulence models together with the presentation of an outlook on future developments.

2. Typical applications in environmental and hydrodynamic research

2.1. Pollutant transport in the urban canopy

This type of study enters within the large framework of *computational wind engineering* (CWE), a discipline that has been progressing since the late 1970s, boosted by its potential to overcome the limitations of earlier simplified physical models such as the *Gaussian models* evoked previously in Section 1. Pollutant dispersion within the atmospheric surface layer encompasses a variety of aspects of vital interest that need to be explored: For example, predicting the transport of contaminants from hazardous releases, analyzing the traffic-induced dispersion (Rafailidis, 2000; Kastner-Klein et al., 1997; Meroney et al., 1999), and studying the effects of neighbouring

building topography on domestic gas-releases (Cowan et al., 1997; Delaunay et al., 1997; Hangan, 1999; Castro et al., 1999). Without considering the thorny question of predicting the behaviour of hazardous gas releases (Chernobyl type of tragedies) to the atmosphere, we could evoke a similar problem that draws less attention, but may nevertheless have an impact on daily life: The quality of air inside a single or a group of buildings and its relation to external aerodynamic conditions. These flow conditions can, for example, connect an external source of pollutants (chimneys releasing exhaust gases from centralized heating devices) with fresh-air admission (windows, etc.) which could in turn be contaminated. Although recent contributions to the field have taken further steps by dealing with dispersion around complex (several buildings) configurations (e.g. Hangan, 1999; Castro et al., 1999), the example selected here consists of the three-dimensional prediction of gas dispersion around an isolated, generic building model placed within a simulated urban canopy studied by Delaunay et al. (1997). The aim of this investigation was to provide architects and civil engineers with sufficient indications regarding the flow structure to help them design a group of buildings in which the recirculation of contaminants through fresh air admissions can be minimized.

2.2. Car-induced pollution in urban areas

Car-induced pollution in urban areas is a serious health concern, in particular within cities [1] featuring many street canyons. Most often building aggregates placed within the atmospheric boundary layer may act as artificial obstacles to the wind and cause stagnant conditions. Experimental and numerical studies of such problems aim in general at predicting the time evolution of pollutant concentrations and their implications for the comfort of pedestrians as a function of geometry and pollutant doses (Mestayer et al., 1993; Sini et al., 1996; Moussiopoulos et al., 1998; Rafailidis, 2000). Previous studies showed the number and arrangement of vortex structures within the street canyon to strongly influence vertical exchange rates. It has also been shown that differential heating of street surfaces can grossly influence the capability of the flow to transport and exchange pollutants (Sini et al., 1996). In particular, differential heating could also shift the in-street flow structure from a single-vortex flow to a flow with several counter-rotating vortices. We report here on the results of a recent simulation, conducted by Theodoridis and Moussiopoulos (2000), of the flow and contaminant transport within a typical street-canyon configuration studied experimentally by Rafailidis (2000). In contrast to earlier studies, a number of interesting and original issues typical for this type of problem have been dealt with by the authors, focusing for example on the determination of the subsequent production of NO_x and ozone.

2.3. Dispersion of marine droplets

The fundamental issues of surface layer meteorology have been reviewed by many specialists, e.g. Högström (1996). More specifically with respect to marine climatology Smith et al. (1996) have made available a complete overview leading to a better understanding of air–sea interaction.

[1] Some Mediterranean cities suffer today because their developers opted in the past for street-canyon type conglomerations seeking for shadow (e.g. Medina and Casbah in North Africa).

The authors review the progress achieved in the study of air–sea interaction over the past three decades and its role in the modelling of the coupled system of ocean and atmosphere. Melville (1996) placed emphasis on the role of surface–wave breaking in air–sea interaction and the subsequent impact of aerosol production and transport. More precisely, it is the impact of marine droplets and aerosols on the heat flux balance that represents the key point in this branch, as discussed by Smith et al. (1996) and Fairall et al. (2000). Indeed, the evaporative droplets are known to distort the normal sensible/latent heat flux balance, whereas in their absence the entire surface moisture flux produces a latent heat loss by the ocean leading to an increase in the salinity at the surface. The central issue here is to understand the contribution of sea spray droplets to the transfer of moisture and latent heat from the sea to the atmosphere. The case study reported in the present review refers to the two-dimensional simulation of the turbulent transport and evaporation of droplets ejected by bursting bubbles within various simulated air–sea boundary layers (Edson and Fairall, 1994; Edson et al., 1996). An integrated Eulerian–Lagrangian strategy was employed to compute the flow, temperature and moisture fields, and the trajectory of each ejected droplet; in particular, the particle trajectories were computed by means of a Markov chain based on the discretization of the Langevin equation for dispersed particles, modified to account for the effects of turbulence, gravity and inertia. This type of Lagrangian technique is presently being employed within the LES framework for other related subjects such as the prediction of pollution dispersion in the atmosphere (e.g. Sorbjan and Uliasz, 1999). Studying the generation, transfer mechanisms and aerosol deposition over the ocean has also been migrating gradually from RANS (e.g. Ling et al., 1980; Burk, 1984) to LES (e.g. Glendening and Burk, 1992), although the Eulerian description is still preferred to the Lagrangian one.

2.4. Impacting hydrometeors on buildings

The deterioration experienced by buildings and monuments is caused in part by the direct impact of hydrometeors and subsequent deposition of moisture on the surface. In contrast to the effects caused by the spectacular impact of heavy hydrometeors such as hail, the more subtle degradations caused by moisture deposited by rain, snow and fog are less well assessed. In these instances, the deposited moisture can cause mechanical disruptions by freezing within fissures or by actually dissolving the materials. In addition, atmospheric pollutants dissolved or suspended in water droplets can be carried to the surface. Once these pollutants have been deposited on the surface, capillarity can transport the moisture and pollutants into the interior of porous materials. This often results in chemical transformations and deterioration deep within these structures. For this class of flow the literature reports on a very limited number of computational investigations; the earlier ones have adopted simplified formulations relating the intensity of driving rains to the free-falling rain intensity and wind speed (e.g. Lacy, 1977; Beguin, 1985; Hilaire and Savina, 1989). More elaborate strategies based upon the Eulerian–Lagrangian approach appeared only recently (e.g. Choi, 1994; Lakehal et al., 1995; Sankaran and Paterson, 1997; Karagiozis et al., 1997). However, the only contribution in this field combining in a single model the effects of turbulence, gravity, and inertia is due to Lakehal et al. (1995). The example reported here (from these authors' work) centers around the prediction of wind-driven raindrop trajectories inside a two-dimensional street canyon; the final aim was to evaluate the impacting water rate on the facades. The solution procedure was again based on an integrated Eulerian–Lagrangian method,

and the particle trajectories were computed by means of a Markov chain modified to account for the effects of turbulence, gravity, and inertia.

2.5. Sedimentation in water clarifiers

Settling and sedimentation phenomena are complex processes, repeatedly evoked in hydrodynamic applications; their presence within wastewater treatment plants as the most important unit operations is one example among various others. It is well known that gravity-induced sedimentation and the subsequent thickening process may be subdivided into four different types: Discrete particle settling, flocculent settling, hindered settling, and compression (see, for example, Karl and Wells (1999) for classification). The thickening process in water clarifiers occurs most often as a combination of the last three forms, which poses challenges to the modeler. The recent critical review of Parker et al. (2001) reports on the important design aspects properly applicable to clarifier technology that need to be observed. Investigating this type of flow is dictated by design interests: It is aimed at helping to design secondary clarifiers, whose efficiency is such that the overall performance of the entire wastewater treatment does not require post operations (Krebs et al., 1996). An intensive scientific effort has recently been made in order to understand this type of flow, and various numerical models have been developed for the purpose, most of which are based on two-equation turbulence models describing the flow pattern and sediment-induced density currents (Lyn et al., 1992; Zhou et al., 1992; Zhou and McCorquodale, 1992; Szalai et al., 1994; Vitasovic et al., 1997; Armbruster et al., 2001). Apart from Lyn et al. (1992) the above cited works did not consider particle decompositions and were thereby based on the determination of an average settling velocity for suspended particles. Jin et al. (2000) have recently taken a step ahead by proposing a one-dimensional model for non-uniform sediment transport capable of handling flocculation, coagulation, and filtration. This type of flow raises additional complexities as compared to pollutant dispersion problems. Buoyancy effects may be more important than those induced by turbulent stresses. The transported phase settles at a velocity strongly influenced by its concentration. Finally, the non-Newtonian behaviour of the activated sludge requires appropriate definition of its rheological properties. The results of modelling the sedimentation of a sludge blanket in a circular, center-fed secondary clarifier with inclined bottom and central withdrawal are presented. Axisymmetry is assumed and the flow and settling processes (with variable settling velocities) are computed in a radial section. The non-Newtonian behaviour of the sludge is also taken into account.

2.6. Bubble plumes

Three-dimensional mixing of multiphase flows may occur in industrial applications as well as in environment protection processes. Industrial applications include gas stirring by liquid metal ladles in several metallurgical processes, or venting of vapour mixtures to liquid pools in chemical and nuclear reactors. Bubble plumes may also be involved in environment protection problems such as the aeration of lakes, mixing of stagnant water and, generally, de-stratification of water reservoirs. For all these applications the basic need is to determine the currents induced by the gaseous phase evolving in the surrounding liquid and thereby to establish the consequent mixing and partition of energy, or species concentration in the body of the liquid. Here the computational

methodology to be followed is the two-fluid approach of Ishii (1975) evoked previously. However, more important is the fact that predicting bubbly flows cannot be achieved without suitable models capable of correctly representing interphase momentum transfer mechanisms and turbulence modulation induced by the bubbles. For the latter issue, various models have been published in the past, though all of them resort to a single-phase two-equation turbulence model modified to account for these exchange mechanisms (Malin and Spalding, 1984). This includes the effect of bubble migration through the liquid (Simonin and Viollet, 1988), and more often the interactions between the eddies and the dispersed phase via what is known as *turbulent dispersion models* (see, for example, Moraga et al., 2001, for a recent review). In practice the idea of turbulence dispersion induced by the dispersed phase has most often been reflected in terms of a superposition of the shear-induced and bubble-induced stress tensors in the equations for the liquid phase; the latter being constructed on the basis of scaling arguments. The example reported here consists of the prediction of a confined bubble plume studied experimentally by Anagbo and Brimacombe (1990). The numerical results reported here were obtained by Smith and Milelli (1998), who made a critical assessment of various models that have so far been advanced to support modelling of bubbly flows.

3. Outline of the solution methods

3.1. The Eulerian–Eulerian one-fluid approach

3.1.1. Background

To handle the transport of a dilute continuum acting as a passive scalar within a turbulent flow one generally resorts to the so-called Eulerian–Eulerian one-field formalism. In this approach the particle concentrations are assumed to have some characteristics of a continuous phase and some characteristics of a dispersed phase via the inertial slip, when appropriate (e.g. when the particles settle). An inherent concept in this formalism is the assumption that the transported (passive or active scalar) phase obeys the same Navier–Stokes equation governing the mean flow, since there is no interfacial or interphase exchange processes to account for. However, in general, the presence of heavy particles with non-negligible inertia raises simulation problems not yet totally resolved, such as the lack of appropriate boundary conditions.

3.1.2. The transport equations

The Eulerian–Eulerian approach is essentially based on the solution of the Reynolds Averaged [2] Navier–Stokes equations (RANS) governing the motion of an incompressible carrier phase (cf. Hinze, 1975), together with a transport equation for the dilute phase:

$$\partial_j \overline{U}_j = 0, \tag{1}$$

$$D_t \overline{U_i} = -1/\rho_w \partial_i \overline{p} + \partial_j\left(\sigma_{ij} - \tau_{ij}\right) + \vec{f}, \tag{2}$$

[2] Hereinafter each barred symbol represents an ensemble average, while primed letters denote the fluctuating counterparts.

$$D_t\overline{C} = \mathscr{D}\nabla^2\overline{C} - \partial_j\overline{u_j'c'}. \tag{3}$$

In the above equations, $D_t = \partial_t + \overline{\mathbf{u}}\cdot\nabla$ stands for the substantial derivative, σ_{ij} the viscous stress, ρ_w the mean density of the fluid at a reference state, $\overline{p}$ the pressure, $\mathscr{D}$ the molecular diffusivity coefficient, and $\tau_{ij} \equiv \overline{u_i'u_j'}$ the Reynolds stress tensor that requires a model. The buoyancy force term, $\vec{f}$, is effective only in thermally stratified flows and/or when the dispersed phase is appreciably heavier than the carrier fluid. For instance, case studies CS1, CS2 and CS5 were treated on the basis of Eqs. (1)–(3), with $\vec{f} = 0$ for the first two examples.

3.1.3. Thermally stratified flows with mass transfer

The presence of an evaporative medium (e.g. marine droplets) within a thermally stratified flow (e.g. a marine sublayer) can be treated on the basis of the RANS equations (1) and (2), using the Boussinesq approximation, in which the buoyancy force term now reads $\vec{f} = -g_i(\Theta_v - \Theta_v^r)/\Theta_v^r$. This term is induced by the difference between the instantaneous virtual potential temperature[3] Θ_v and that of the reference state Θ_v^r. According to Stull (1988), the presence of water droplets requires the virtual potential temperature to conform to the following relation

$$\Theta_v = \Theta[1 + 0.61q_V - q_L - q_D], \tag{5}$$

in which q_L is the specific humidity of the liquid, and q_D the contribution to the total specific humidity from the droplets to be determined by integrating the local droplet volume concentration. At high-Reynolds numbers the thermal and moisture fields are represented by the Reynolds averaged transport equations for the potential temperature Θ and the total specific humidity denoted: $\mathscr{Q} = q_V + q_L$

$$D_t\overline{\Theta} = -\partial_j\overline{u_j'\theta} + L_E S_q/C_p, \tag{6}$$

$$D_t\overline{\mathscr{Q}} = -\partial_j\overline{u_j'q} + S_q. \tag{7}$$

In these equations C_p stands for the specific heat at constant pressure, L_E for the latent heat of vaporization, and S_q for the total evaporation rate. The reader can refer to Pruppacher and Klett (1978) for more details on the modelling of the source term S_q. Note that the molecular diffusion contributions in the above equations have been dropped, since only high-*Re* number flows are of interest in these studies. The turbulent fluxes $\overline{u_j'q}$ and $\overline{u_j'\theta}$ appearing in Eqs. (6) and (7) need to be modelled, too, as will be discussed later.

3.1.4. Density-induced stratification in non-newtonian mixtures

In certain class of flow the dense phase deposited over an impermeable surface forms a structure behaving like a non-Newtonian material. This is the case for biological material settling in water clarifiers. In a similar context, with use of the Boussinesq approximation the momentum equations take the form of Eqs. (1) and (2), but the buoyancy force is now driven by the difference

[3] The equation of state for "humid air", a mixture of dry air and water vapor, is:

$$p = \rho_a R_a \Theta + \rho_V R_V \Theta = \rho_a R_a \Theta_v; \quad \Theta_v = \Theta[1 + 0.61q_V], \tag{4}$$

where Θ stands for the potential temperature, q_V for the specific humidity of water vapor, and 0.61 is the explicit value of $(R_V - R_a)/R_a$.

between the densities of dry particles and clear water, i.e. $\vec{f} = -g_i\overline{C}(\rho_p - \rho_w)/\rho_p$. The convection–diffusion equation for the field of suspended solids concentration $\overline{C}$ has the form of Eq. (3). However, in order to describe the particle settling process (with or without sedimentation) the convective process in this equation must be augmented by the gradient of the settling flux $F_s = (\rho_w W^s \overline{C})$ in the gravity direction, where W^s denotes the particle settling velocity. It the case of falling water-droplets W^s is conventionally made proportional to the Stokes velocity. In the context of case study CS5, however, this process was modelled using the double-exponential settling function of Takàcs et al. (1991)

$$W^s = W^{s0}\left[e^{-C_a C} - e^{-C_b C}\right], \tag{8}$$

in which the coefficients C_a and C_b are subject to calibration depending on the case studied, and W^{s0} is the settling velocity of reference.

The constitutive equations for the total stress $\sigma_{ij} - \tau_{ij}$ in Eq. (2) must reflect the thermodynamic state of the fluid mixture. When the mixture does not behave like a Newtonian material, adequate rheological properties have to be incorporated. For example, the rheology of activated sludge (case study CS5) was incorporated according to Dick and Ewing's (1967) recommendations, i.e. the plastic behaviour of the sludge requires a Bingham approach. Lakehal et al. (1999) synthesized all these properties, including the closure for the shear-induced turbulence, in the following generalized constitutive expression:

$$\sigma_{ij} - \tau_{ij} = \left[\tau_b/S + 2\left(\mu_p + \mu_t\right)\right]S_{ij}; \quad S = 2(S_{ij}S_{ij})^{1/2}, \tag{9}$$

where the yield stress τ_b and the plastic viscosity of the fluid mixture were approximated by $\tau_b = \beta_1 e^{(\beta_2 C)}$ and $\mu_p = \mu + 2.473 \times 10^{-4}\ C^2$. The coefficients β_1 and β_2 were determined by extrapolating the experimental data of Dahl et al. (1994), yielding $\beta_1 = 0.00011$ and $\beta_2 = 0.98$. In Eq. (9), μ_t denotes the eddy viscosity accounting for the contribution of turbulence to the diffusive processes in the momentum equations (see Section 3.3.1).

3.2. The Eulerian–Eulerian two-fluid approach

3.2.1. Background

This is an alternative route to model multicomponent fluids, also known as the *interpenetrating media formalism* (IMF) or the *continuum formulation* (CF) of Ishii (1975). It assumes that the phases present in the system behave like a continuum. The method can be employed either for mixtures of immiscible fluids, such as bubbly flows, or for dispersed flows involving the presence of small-scale entities such as micro bubbles, droplets and particles. The volume averaged transport equations are in essence similar, and reflect the interpenetration of phases resulting from interfacial forces. A conceptual clarification is necessary at this stage: The volume averaging in question (referred to as *phasic averaging*) is needed for the development of the instantaneous equations describing the present components as continuum; a further averaging (Reynolds or Favre averaging, to which we will refer as *turbulence averaging*) is then performed in order to define quantities for each phase analogous to Reynolds stresses. Generally, using the IMF, separate conservation equations are required for each phase, together with interphase exchange terms, and, where appropriate, extra equations for turbulence modelling. In the absence of mass or heat transfer between the phases no energy equation is needed, and a turbulence model is

required for both phases, even if the turbulent stress tensor appearing in the momentum equations of the gas phase is less important than in the liquid phase [4].

3.2.2. The transport equations

Although the instantaneous phasic averaged equations can be formulated differently (e.g. Ishii, 1975; Lahey and Drew, 1988; Besnard and Harlow, 1988; Joseph et al., 1990; Drew and Passman, 1999), in the volume-average formulation (e.g. Elghobashi, 1994; Lance and Bataille, 1991) the (arbitrary) volume over which the *phasic averaging* is performed should be larger than the characteristic length scale of the dispersed phase (e.g. bubble diameter, particle spacing) and much smaller than the characteristic length of the problem. The *turbulence averaging* to be performed on top of the phasic averaged equations may be either a non-weighted time average or a Favre weighted average based on α^k, the volume fraction [5], defined as $\alpha^k = \overline{\chi}^k$; with χ^k (=1 in phase k, and 0 otherwise) being the characteristic function of phase k, i.e. the fraction of occurrences of phase k at point $\mathbf{x}$ at time t. Once adopted, Reynolds averaging ($\Phi = \overline{\Phi} + \phi'$) gives rise to two correlations $\overline{\alpha' u_j'}$ and $\overline{\alpha' u_i' u_j'}$, respectively, in the continuity and momentum equations; the gradient of the flux $\overline{\alpha' u_j'}$ is responsible for mass diffusion in the continuity equation. These terms require appropriate modelling (cf. Elghobashi and Abou-Arab, 1982; Shirolkar et al., 1996; Loth, 2001). In order to alleviate this complication, preference is often given to Favre weighted averaging ($\overline{\Phi} = \overline{\Phi\alpha}/\overline{\alpha}$), in which case the correlations $\overline{\alpha' u_j'}$ and $\overline{\alpha' u_i' u_j'}$ are identically zero.

In these circumstances, for an isothermal gas–liquid mixture without phase change the (twice) averaged transport equations can be formulated as follows:

$$\partial_t\left(\alpha^k \rho^k\right) + \partial_j\left(\alpha^k \rho^k \overline{U_j}^k\right) = 0; \quad \sum \alpha^k = 1, \tag{10}$$

$$D_t\left(\alpha^k \overline{U_i}^k\right) = -\frac{\alpha^k}{\rho^k}\partial_i \overline{p}^k + \partial_j\left(\alpha^k \sigma_{ij}^k - \alpha^k \tau_{ij}^k\right) + \alpha^k g + F_j^k, \tag{11}$$

where the superscript k refers either to the liquid ($k = l$) or to the gas phase ($k = g$). The source term F_j^k encompasses the drag and lift forces, the added mass, and the turbulent dispersion force (TDF). A detailed description of the involved forces can be found in Smith (1998); below, we simply describe the way these terms are generally incorporated into the system of equations.

The buoyancy forces can be imposed as extra source terms in the momentum equations, and so can the treatment for the virtual mass. While for rigid spheres the virtual mass coefficient is $C_{vm} = 0.5$, there is no clear indication yet regarding the corresponding value for a rising bubble swarm. Nevertheless, as a consensual solution the value of 0.5 was adopted in the past by many authors, with the exception of Smith and Milelli (1998), who investigated the effect of varying C_{vm} in the case of a confined bubble plume; see Section 4.6 (Table 1). Note that the virtual mass force is important during the early accelerating phase of bubble-plume development but becomes less important as steady-state conditions are approached. According to Davidson (1990), the

[4] In practice the stress tensor in the gaseous phase equations is simply neglected, and a turbulence model is only required for the liquid phase.

[5] Note that rigorously α^k is the ratio of the volume of component k in an arbitrary small region to the total volume of the region in question.

interphase drag force can be derived from a generalization of that for a single bubble, and a drag coefficient set equal to $C_D = 0.44$ may be considered as appropriate for small air bubbles rising in pure water. In addition, an ascending gaseous phase within a pool of water causes horizontal shear, which in turn generates a lateral lift force acting on the rising bubbles; according to Drew and Lahey (1987) the lift coefficient can be taken equal to $C_L = 0.5$.

The concept of a TDF has already been advanced as an approximation to the random interaction between eddies and bubbles (Lopez de Bertodano et al., 1994; Moraga et al., 2001). Another approach, called the *random dispersion model* (RDM), has recently been proposed by Smith and Milelli (1998). This strategy dispenses entirely with the aforementioned artificial turbulent dispersion models by incorporating the statistical, turbulent fluctuations in the liquid directly into the expressions for the drag. It assumes that the fluctuating velocity components are random deviates of a Gaussian distribution with zero mean and variance $2k^l/3$. More details can be found in Smith and Milelli (1998).

3.3. Turbulence modelling

As pointed out in Section 1, all case studies reviewed in this article enter within the turbulence modelling framework. In this section we briefly present the various turbulence models that have been employed without exploring in depth their mathematical formalism, except when buoyancy effects significantly alter the closure law. In all cases the turbulent stresses and scalar fluxes τ_{ij} (Eqs. (2) and (11)), $\overline{u_j'c'}$ (Eq. (3)), $\overline{u_j'\theta}$, $\overline{u_j'q}$ (Eqs. (6) and (7)) have to be approximated via closure laws. In the case where Eqs. (10) and (11) are derived via non-weighted time averaging the correlations $\overline{\alpha' u_j'}$ and $\overline{\alpha' u_i' u_j'}$ require modelling as well (Shirolkar et al., 1996; Loth, 2001).

3.3.1. Within the one-fluid approach

In the context of case study CS1 the Reynolds stress tensor τ_{ij} was modelled with the aid of a second moment closure (SMC), in which the Launder et al. (1976) proposal for the pressure strain term and the Gibson and Launder (1978) *wall reflection* terms were adopted. Within the SMC framework, the scalar flux $\overline{u_j'c'}$ (Eq. (3)) was modelled using the *generalized gradient diffusion hypothesis* (GGDH) by reference to the Daly and Harlow (1970) approximation. Since the aim of that work was to elucidate the effect of turbulence anisotropy on gas dispersion around the building, the flow was additionally calculated with the standard k–ϵ model of Launder and Spalding (1974) and a zonal two-layer approach, consisting in resolving the near-wall viscosity-affected regions by means of a one-equation model, while the outer core flow is resolved with the standard model (cf. Lakehal and Rodi, 1997). Modelling of the scalar flux naturally followed the eddy-viscosity/diffusivity (EVM) context in which the flux is made proportional to the mean gradient of the variable in question.

The flow field within the street canyon (due to Theodoridis and Moussiopoulos, 2000), i.e. case study CS2, was computed with the help of the standard k–ϵ model and the two-layer k–ϵ model briefly mentioned above. Furthermore, a fast chemical reaction model based on the NO–NO_2–O_3 cycle permitted the determination of the subsequent production of NO_2, NO_x, and O_3 within the street canyon. The turbulent stresses and fluxes emerging in the context of examples CS3, CS4, CS5, and CS6 were also modelled by use of the EVM concept.

In the case studies referred to as CS3 and CS5 the effect of the buoyancy-induced turbulent flux emerges in the transport equations for k and ε

$$D_t k = \partial_i\left(\frac{\nu_t}{\sigma_k}\partial_i k\right) - \tau_{ij}\overline{U}_{i,j} + P_B - \varepsilon, \tag{12}$$

$$D_t \varepsilon = \partial_i\left(\frac{\nu_t}{\sigma_\varepsilon}\partial_i \varepsilon\right) + C_1\frac{\varepsilon}{k}\left(-\tau_{ij}\overline{U}_{i,j} + P_B - C_3 P_B\right) - C_2\frac{\varepsilon^2}{k} \tag{13}$$

via the production term P_B, which takes the form $P_B = -\beta g\overline{u_j'\theta_v}$ in the thermally stratified flow (CS3), and $P_B = -\beta g\overline{u_j'c'}$ in the sedimentation case (CS5), respectively. In Eqs. (12) and (13) the σ's and C_1, C_2, and C_3 are model constants. The density-induced production term P_B represents in a certain manner the two-way coupling between the dense phase and the liquid. The model expresses the eddy viscosity ν_t as a function of the turbulent kinetic energy k and its rate of dissipation ε, using the relation $\nu_t = C_\mu k^2/\varepsilon$. The scalar flux $\overline{u_j'c'}$ was approximated with use of an eddy diffusivity concept. However, in the marine boundary layer, the buoyancy-induced turbulent flux $\overline{w'\theta_v}$, including all sources of moisture, was approximated following Stull's (1988) recommendation:

$$\overline{w'\theta_v} = \overline{w'\theta}\cdot\Theta_v + \Theta\left[0.61\overline{w'q_V'} - \overline{w'q_L'} - \overline{w'q_D'}\right]. \tag{14}$$

The turbulent fluxes $\overline{w'q_V'}$, $\overline{w'q_L'}$, and $\overline{w'q_D'}$ were also approximated using the EVM concept, with the Schmidt number Sc taken equal to 0.95 in all cases.

In modelling density stratified flow mixtures in particular, e.g. case study CS5, one may face the problem of fixing the model coefficients appearing in Eq. (13). While model constants C_μ, C_1 and C_2 may be given the well-established standard values, the magnitude of C_3 must be taken as flow dependent. Test calculations have shown that the value of C_3 depends on whether P_B is a source term (in the case of unstably stratified flows) or a sink term (in the case of stably stratified flows). Rodi (1987) suggested that C_3 should fall in the range 0.8–1.0 for stable stratification prevailing in secondary clarifiers. But, according to Shabbir and Taulbee (1990), there has been experimental evidence that C_3 falls within a lower range, in particular for strongly buoyant flows, where in some cases it was found to attain values converging around 0.25. Although the consensual value of $C_3 = 0.8$ has been adopted by many authors for similar problems (e.g. Dahl et al., 1994), it is perhaps more judicious to study its influence in the context of k–ϵ modelling (see Section 4.5). Since in case study CS3, P_B is a source term, C_3 was taken equal to zero.

3.3.2. Within the two-fluid approach

The k–ϵ model employed so far within the two-fluid formulation context (Lopez de Bertodano et al., 1994; Lahey and Drew, 2001) has been the subject of various developments. The major issue was the incorporation of two-way coupling effects, because turbulence in the liquid phase has a strong influence on the void fraction distribution and bubble flattening, while fragmentation and wobble will have feedback effects on the production of turbulent kinetic energy (Sheng and Irons, 1993). Various alternatives have been proposed to account for this dispersion mechanism (see Moraga et al., 2001). For example, Lopez de Bertodano et al. (1994) introduced a TDF proportional to the Reynolds stress tensor of the dispersed phase and a scalar coefficient dependent on the Stokes number. Drew and Passman (1999) and Carrica et al. (1999) proposed to make this

force proportional to the gradient of the void fraction in the momentum equations of the dispersed phase, in analogy to molecular Brownian diffusion. Another solution consists in adding extra source terms to the scalar equations for turbulence, k and ε, to account for the increased generation of turbulence in the liquid due to momentum exchange between the two phases (Malin and Spalding, 1984). In addition, Simonin and Viollet (1988) argued that the migration of bubbles has an important effect that cannot be neglected.

Typically, at high-Reynolds numbers the system of turbulent scalar equations for the liquid phase takes the form:

$$D_{\mathrm{t}}(\alpha^l k) = \partial_i\left(\frac{\tilde{\nu}_{\mathrm{t}}}{\sigma_k}\partial_i k\right) + \alpha^l(P_k - \varepsilon) + C_{k1}\tilde{\alpha}P_k + C_{k2}C_{\mathrm{f}}\tilde{\alpha}k, \tag{15}$$

$$D_{\mathrm{t}}(\alpha^l \varepsilon) = \partial_i\left(\frac{\tilde{\nu}_{\mathrm{t}}}{\sigma_\varepsilon}\partial_i \varepsilon\right) + \alpha^l \frac{\varepsilon}{k}(C_1 P_k - C_2\varepsilon) + C_{\varepsilon 1}\tilde{\alpha}P_k\frac{\varepsilon}{k} + C_{\varepsilon 2}C_{\mathrm{f}}\tilde{\alpha}\varepsilon, \tag{16}$$

where $P_k = -\tau_{ij}^l U_{i,j}^l$ represents the shear-induced production of turbulent kinetic energy, $\tilde{\alpha} = \alpha^g\alpha^l$, $\tilde{\nu}_{\mathrm{t}} = C_\mu \alpha^l k^{l^2}/\varepsilon^l$, and C_{f} is the interface friction coefficient. In the above equations, C_{k1}, C_{k1}, $C_{\varepsilon 1}$, and $C_{\varepsilon 2}$ represent additional model coefficients which, according to Smith (1998), take the values of 6.0, 0.75, 4.0, and 0.6, respectively. The first additional source terms in Eqs. (15) and (16) are due to Malin & Spalding (MS); the last ones conform to the proposition of Simonin & Viollet (SV).

3.4. The Eulerian–Lagrangian formalism

3.4.1. Background

The principle of the Eulerian–Lagrangian strategy resides in the coupling between an Eulerian field description algorithm for the steady-state flow solution and a Lagrangian scheme for tracking individual particles within this flow field. The simulation of IP trajectories subjected to gravitational force conventionally resorts to the equation of motion for spherical particles (Clift et al., 1978). Subjecting the particle motion to the field turbulence requires the fluctuating velocity field to be known (i.e. modelled). Existing dispersion models differ in the way this fluctuating field is stochastically inferred from known turbulence quantities. Moreover, properties of heavy particles such as inertia and (for example) gravity-induced settling velocity need also to be considered. To this end, models of various degrees of sophistication accounting for the influence of these properties on the statistics of particle motion were proposed on the basis of theoretical studies (e.g. Csanady, 1963; Meek and Jones, 1973) and on experimental grounds (e.g. Snyder and Lumley, 1971; Wells and Stock, 1983). However, DNS and LES experiments such as those referred to in Section 1 have not yet been fully exploited for similar objectives. The work of Csanady (1963), for example, helped understand the effect of slip velocity on the dispersion of IPs with zero-settling velocity. Wells and Stock (1983) raised the question of *crossing-trajectory* events caused by the combined effects of inertia and gravity forces. These two issues are at the basis of the random-flight models discussed in this part. The next three subsections will introduce the particle momentum equation, two of the often employed random-flight models and their recent developments, and finally the way a typical coupled Eulerian–Lagrangian simulation proceeds.

In principle, the Eulerian part of this approach consists in solving Eqs. (1) and (2). Applications including temperature and specific humidity fields require in addition the solution of Eqs. (6) and (7). This is particularly true for CS3, while the example of impacting rain drops (CS4) was approached under isothermal conditions. Turbulence equations similar to (12) and (13) were solved, with $P_B = 0$ in case study CS4.

3.4.2. The particle momentum equation

The two different Lagrangian models introduced below are based on the equation of motion for a spherical particle in high-Reynolds number flows (cf. Clift et al., 1978):

$$d_t X_i^p = U_i^p, \tag{17}$$

$$d_t U_i^p = \frac{3}{8r}\frac{\rho_w}{\rho_p} C_D U_i^r |U_i^r| + g_i \frac{\rho_w}{\rho_p}\left[\left(\frac{\Delta_a}{2} D_t U_i - d_t U_i^p\right) + \frac{9\Delta_h}{2r}\sqrt{\frac{\nu}{\pi}}\int_{t_0}^{t} D_{t'} U_i^r \frac{dt'}{\sqrt{t-t'}}\right], \tag{18}$$

where U^p and U^r are the instantaneous particle velocities in the fixed co-ordinate system, and in the relative co-ordinate frame following the fluid motion, respectively, i.e. $U_i^r = U_i - U^p$; X_i^p are the instantaneous particle co-ordinates, C_D is the drag coefficient for a spherical particle, ρ_p is the mean density of the dispersed phase, and Δ_a and Δ_h are empirical correction coefficients introduced by Clift et al. (1978). In Eq. (18), terms on the right represent, respectively, the viscous resistance to particle motion, the gravitational acceleration, the added mass which appears because the particle acceleration also requires acceleration of the fluid, the acceleration due to the pressure gradient in the fluid surrounding the particle, and the "Basset history integral", accounting for past accelerations in non-steady-state flow, where t and t' represent, respectively, initial and present times of particle motion. Note that both the Saffman and Magnus effects have been neglected. Since the particles are supposed to be smaller than Kolmogorov's micro-scale, heavy (e.g. $\rho_p/\rho_w \sim 10^{-3}$), spherical, and of Reynolds number always less than unity, so that the resistance of the fluid obeys Stokes' law, Eq. (18) can be simplified to:

$$d_t U_i^p = \frac{K}{\alpha}|U_i^r| + g_i, \tag{19}$$

where the drag and gravity terms are the only effective forces acting on the particle. The parameter $\alpha/K \equiv \tau_p$ characterizes the time scale of the particle's inertial response to the turbulent fluctuations of the fluid, i.e. the particle relaxation time. Note that in case studies CS3 and CS4, U^r was set to zero, assuming horizontally homogeneous flows. The vertical particle velocity is given by $W^r = -W^s$ for particles of diameter smaller than 60 μm and $W^r = -W^s/K$ for particles of diameter 60–180 μm, where W^s denotes the Stokes velocity. According to Clift et al. (1978), K, the ratio of the Stokes velocity to the mean relative fall velocity of the particle, adheres to the relation $K = 1 + \gamma_1 Re_p^{\gamma_2}$ for the drag coefficient, [6] in which γ_1 and γ_2 depend on the particle Reynolds

[6] This way of expressing τ_p is due to Edson (1989). One can easily demonstrate that $K = C_D(Re^p/24)$, $\alpha = \rho_p D^2/18\mu_w$, $W^s = \alpha g$ and $Re_p = \rho_w W^s D/K\mu_w$. Note also that Choi (1994) employed the distribution of drag coefficients for falling water droplets measured by Gunn and Kinzer (1949). Lakehal et al. (1995) extended the expression to high-Re particles.

number, Re_p. Further, it is assumed that the particle motion is in a quasi-steady state, so that the particle velocity consists of the mean free-falling velocity plus a fluctuating component,

$$W^{\mathrm{p}}(t) = \overline{W^{\mathrm{p}}} + w^{\mathrm{p}} = \overline{W}(\mathbf{x}^{\mathbf{p}}, \mathbf{t}) - W^{\mathrm{r}} + w^{\mathrm{p}}, \tag{20}$$

where $\overline{W}(\mathbf{x}^{\mathbf{p}}, \mathbf{t})$ is the mean velocity of the fluid at the particle location, and w^{p} is the fluctuating component which needs to be known.

3.4.3. Markov chain based algorithms (F1)

A Markov-chain sequence is a time-marching process integrating the finite discrete form of the Langevin equation [7] that formally describes the motion of small-scale fluid entities (i.e. particles, droplets, or fluid elements) as a stochastic process subject to a retarding force and a random acceleration (Lin and Reid, 1962)

$$\mathrm{d}w = -aw\,\mathrm{d}t + b\xi(t), \tag{21}$$

where $w(t)$ is the particle or fluid element single velocity component. $\xi(t)$, which is not a function of w, reflects the rapidly fluctuating acceleration induced by forces exerted by the turbulence on fluid particles during $\mathrm{d}t$. It is modelled as a delta-function correlated in time with statistical properties defined by (van Kampen, 1992):

$$\overline{\xi^n(t)} = \overline{\xi(t_1)\xi(t_2)\cdots\xi(t_n)} = \Gamma_n\delta(t_1 - t_2)\cdots\delta(t_1 - t_n), \tag{22}$$

where $n = 1, 2, \ldots$, and Γ_n are coefficients to be determined. Consistency between Eq. (21) and those representing the mean flow was addressed by many authors (MacInnes and Bracco, 1992). In particular, it is required that the two forms should return identical statistical properties for the particle motions when these are interpreted as fluid elements. This consistency, for instance, has been proved (Pope, 1987) for homogeneous isotropic turbulence, in which case the first through third-order moments defined by Eq. (22) reduce to $\overline{\xi(t)} = 0$, $\overline{\xi(t)^2} = 2\sigma_w^2\mathrm{d}t/\tau_w$ and $\overline{\xi(t)^3} = 0$, where σ_w^2 is the variance of the turbulence velocity and τ_w is the Lagrangian time scale. Under these circumstances it can be shown (Legg and Raupach, 1982) that the unknown coefficients in Eq. (21) can be determined by $a = 1/\tau_w$ and $b = \sigma_w\sqrt{2a}$. Eq. (21) has been applied by Thomson (1971), Hall (1975), Reid (1979) and many others to particle dispersion in the surface layer assuming homogeneous turbulence. However, in its present form it cannot be extended to atmospheric diffusion without further modifications. Legg and Raupach (1982) and Legg (1983) added an extra term to the basic equation equivalent to a non-zero mean random forcing $\overline{\xi(t)} \neq 0$. De Baas et al. (1986) modified the first and second-order moments of $\xi(t)$. Recently, Nasstrom and Ermak (1999) developed a homogeneous Langevin equation model in which higher background velocity moments up to $\overline{\xi^6(t)}$ were taken into account. They have clearly shown that this form is significantly more efficient than earlier ones. Beyond the concept discussed above, Pope (1994) reformulated the Langevin equation in terms of instantaneous velocities and introduced the mean pressure gradient to cope with non-homogeneous turbulence. This offers a major advantage in that the separation between mean and fluctuating velocity fields is no longer necessary.

[7] Its equivalent in the Eulerian frame is the Fokker–Plank equation. It is also known as the Ornstein–Uhlenbeck process.

The model variant (referred to as F1) employed for case studies CS3 and CS4 was developed by Edson (1989) for the modelling of evaporating jet droplets. It was later modified by Lakehal et al. (1995) for dispersion of hydrometeors in the surface layer. A similar technique was previously employed by Durbin (1980) for dispersion in inhomogeneous turbulence. In this model Eq. (19) is used to determine the statistical properties of particle motion whereas the Langevin equation in the above-described form (valid for stationary, homogeneous turbulence) is introduced to model the fluctuating particle velocities,

$$\mathrm{d}w^{\mathrm{p}} = -\frac{w^{\mathrm{p}}}{\tau_{wp}}\,\mathrm{d}t + \left(\frac{2\sigma_{wp}}{\tau_{wp}}\right)^{1/2}\xi(t), \tag{23}$$

where τ_{wp} now stands for the particle or droplet integral time scale, σ_{wp} is the standard deviation of the particle's velocity variance, and $\xi(t)$ is a random function with a Gaussian probability density distribution, a zero mean, and with $\xi(t_1)$ and $\xi(t_2)$ independent for $t_1 \neq t_2$. At this stage the model still lacks expressions for τ_{wp} and σ_{wp} which, within the one-way coupling context, need to be evaluated from their Eulerian counterparts. There have been different proposals for approaching this *similarity* problem within the heavy particle limit: Edson (1989) and Edson and Fairall (1994) related the energy spectral density of the particles with zero settling velocity to the fluid spectral density then included the effect of non-zero settling velocity as suggested by Meek and Jones (1973). This led to the following expression:

$$\frac{\sigma_{wp}^2}{\sigma_w^2} = \frac{1}{1+c\chi}; \quad \chi = \frac{\alpha}{K\tau_{\mathrm{L}}} = \frac{\tau_p}{\tau_{\mathrm{L}}}, \tag{24}$$

which is the exact form proposed by Tchen (cited by Hinze, 1975) for IPs (with no external forces) dispersed in isotropic turbulence. The parameter χ, denoting the ratio of the response time of the particle or droplet to the Lagrangian integral time scale τ_{L}, guarantees that the particles cannot respond to the turbulence for values of χ larger than unity, e.g., when the particles encounter smaller eddies or near the wall. The effect of varying the value of constant c (taken equal to unity in the F1 model) is discussed by Wilson (2000). Furthermore, the presence of an external force such as gravity induces a crossing-trajectory effect which can best be parametrized by the ratio of characteristic velocities $W^{\mathrm{r}}/\sigma_{wp}$. The same arguments employed by Edson and Fairall (1994) to derive Eq. (24) led to an analytical correction for τ_{L}, i.e the particle integral time scale τ_{wp}, that includes precisely the effect of the gravity-induced drift through

$$\frac{\tau_{wp}}{\tau_{\mathrm{L}}} = \frac{1}{\Lambda}(1+\chi); \quad \Lambda = \sqrt{1+\gamma^2\left(W^{\mathrm{r}}/\sigma_{wp}\right)^2}. \tag{25}$$

This expression reduces to the form proposed by Csanady (1963) if one takes $\chi = 0$ and $\gamma = \tau_{\mathrm{L}}/\tau_{\mathrm{E}}$, where τ_{E} denotes the Eulerian time scale. The non-dimensional number γ, which depends on whether the velocity component is parallel or perpendicular to the external force (Sawford and Guest, 1991; Pozorski and Minier, 1998), was set equal to unity in the F1 model. The correction factor $1/\Lambda$ in Eq. (25) reflects the de-correlating effect of the particle falling out of a fluid eddy in which the fluctuating velocities are highly correlated. Together with χ, the parameter Λ accommodates the reduction of the general expressions for particle velocity variance and integral time scale to their equivalents for the fluid parcels as the particle radius tends to zero; they also include

the effect of particles larger than those obeying Stokes' law through the parameter K. The system of Eqs. (23)–(25) can then be closed, provided the turbulence statistics of the carrier phase expressed in terms of τ_L and σ_w are known. Using the output of the k–ϵ model (for example) calibrated for atmospheric and marine surface layers these two parameters are, respectively, given by $\tau_L = \beta k/\varepsilon$ and $\sigma_w^2 = 1.69 C_\mu^{1/2} k$ according to Mestayer et al. (1990). Depending on the experiment referred to the values assigned for β may range [8] from 0.11 to 0.6 (see, for example, Ley, 1982; MacInnes and Bracco, 1992; Shirolkar et al., 1996, for reviews). Recent DNS of Lagrangian statistics in uniform shear flow of Sawford and Yeung (2001) have brought new insight into this issue.

Next, equating the discrete form of Eq. (23) to the discretized form of Eq. (19) yields the instantaneous particle velocity field $W^p(t)$ which, with the aid of Euler's first-order time-marching process provides the particle trajectories. The time step is made equal to the smallest of $0.2\tau_L$, $0.2\tau_{wp}$, and τ_{gr}; the latter constraint denotes the local grid-characteristic time scale and was introduced by Lakehal et al. (1995) to avoid having the particles crossing more than one grid cell in the course of a single integration.

3.4.4. Random eddies based algorithms (F2)

This concept (subsequently referred to as F2) is based on the same assumptions as the Langevin-equation-based model F1, i.e. Eq. (19), but differs in the computation algorithm for particle velocities. The variant discussed here (used for case study CS4) belongs to the class of *eddy interaction models* of Gossman and Ioannides (1981) evoked previously in Section 1. Modelling the velocity fluctuating field perceived by particles along their trajectories is based here on the generation of random eddies from the modelled turbulence field with which individual particles are continuously interacting. The particle velocity remains constant during each particle–eddy interaction time, while the eddy velocity remains unchanged till the next interaction process. The fluctuating components $u_i'(t)$ of the instantaneous fluid velocity are determined randomly from an isotropic Gaussian distribution with a variance equal to $2k/3$. The PDF, for example, of the third component ($i = 3$) reads

$$P(w') = \frac{1}{\sqrt{2\pi}\sqrt{2k/3}} \exp\left[-\frac{w'^2}{4k/3}\right]. \tag{26}$$

The characteristic size of a specific eddy "crossed" by a particle is generated by reference to the dissipation length scale $\ell_e = C_\mu^{3/4} k^{3/2}/\varepsilon$. Proper model usage therefore relies on the choice of an appropriate "correlation time" τ_c, during which the fluid correlation is effectively equal to unity, i.e. the time over which the particle velocity can be assumed to be constant. In order to account for crossing-trajectory effects, τ_c can be chosen to be the smallest of the local values of the par-

[8] It was taken equal to 0.11 for the atmospheric surface layer by Lakehal et al. (1995) and to 0.18 for the marine sublayer by Edson et al. (1996). In reality, β results from the analogy between the Lagrangian velocity structure function determined from Eq. (21), $D(\mathrm{d}t) = [w(t+\mathrm{d}t) - w(t)]^2 = (2\sigma_w/\tau_L)\,\mathrm{d}t$, and the one derived from the Kolmogorov theory of local isotropy, according to which $D(\tau) = C_0 \varepsilon(t) \tau$ exhibits an inertial subrange in the interval of scales τ ranging from the Kolmogorov time scale τ_η to τ_L. It follows that $\tau_L = \beta k/\varepsilon$, where $\beta = 4/3C_0$.

ticle's residence time within the eddy τ_r and the lifetime (or eddy turnover) of the specific eddy τ_e. These can be determined (for a single component velocity field, say W) by

$$\tau_r = \ell_e/|W^r(t)| = \ell_e/|\overline{W} + w'(t) - W^p(t)|; \quad \tau_e = \ell_e/|w'(t)|. \tag{27}$$

The first time scale is a measure of the minimum time it would take a particle to cross an eddy with characteristic dimension ℓ_e; the second one refers to the lifetime of the eddy in question. If τ_c estimated from Eq. (27) is smaller than the eddy lifetime, the particle would jump to another eddy, which then causes a discontinuity in the perturbation field u_i'. This means that a particle may not remain trapped inside an eddy for the entire lifetime of that eddy if the free falling velocity of the particle is significant enough to precipitate the migration to another eddy. Since the relative velocity $W^r(t)$ is unknown during the next particle–eddy interaction time it can be approximated by the one at the beginning of the new interaction. Even though the original approach as described above has proven efficient in treating various dilute turbulent two-phase flows, several analyses have shown the existence of intrinsic drawbacks. First, various other expressions for τ_r were proposed in the literature to allow the model to account for the possibility of finite-inertia particles dispersing faster than the fluid particles (cf. Shirolkar et al., 1996; Graham, 1998; Chen, 2000). To account for turbulence anisotropy Zhou and Leschziner (1991) redefined the correlation time τ_c as a tensor by including individual Reynolds stress components rather than its trace (k), i.e. $\tau_{cij} = C_\tau(k^2/u_i'^2u_j'^2)^{1/4}k/\varepsilon$. This is conceptually more rigorous and advantageous when a second order closure for turbulence solving for individual stress components is adopted. In the same context, another possibility would be to include the normal Reynolds stresses only while sampling the fluctuating velocities or velocity variances.

The importance of accounting for turbulence inhomogeneity was discussed by MacInnes and Bracco (1992) and recently by Chen (2000). This is important, since by assuming constant sampled fluctuating velocities during each particle–eddy interaction time the original model tends to exaggerate the rate of turbulence transfer from high- to low-turbulence intensity regions. MacInnes and Bracco (1992) found that in the non-inertial tracer limit, particles concentrate where the turbulence intensity is a minimum (at shear layer edges), and are depleted in regions of high-turbulence intensity (near the core of the shear layers).

The assumption of streamwise quasi-homogeneity of the flow was invoked in both case studies CS3 and CS4. Regarding this simplification, Lakehal et al. (1995) attempted to extend this model to non-homogeneous flows by generating the horizontal fluctuating component (this latter model will subsequently be denoted by F3). They showed that the correlation between the horizontal and vertical fluctuating velocities can be constructed such that

$$w'(t) = \sigma_w\xi_1(t), \tag{28}$$

$$u'(t) = \sigma_u\xi_2(t)R_{uw} + \sigma_w\xi_3(t)\sqrt{1 - R_{uw}^2}, \tag{29}$$

$$R_{uw} = \frac{\overline{u'w'}}{\sigma_u\sigma_w}, \tag{30}$$

where R_{uw} denotes the autocorrelation factor and $\xi_1(t)$, $\xi_2(t)$ and $\xi_3(t)$ are random numbers drawn from three independent Gaussian distributions $P(u_i')$ given by Eq. (26) with zero mean and unity variance.

Finally, in an application the random-flight tracking algorithms F1 and F2 proceed as follows: During each correlation time the particle is advected N time steps ($\Delta t = \tau_c/N$), and the particle's instantaneous velocity and position are determined by integrating Eq. (19) over τ_c, using an Adams-Bashforth time-marching scheme. The process is repeated until the particle moves to the walls or out of the calculation domain, with no particle–wall impact model employed.

4. Computational examples

This part of the paper introduces the selected computational examples regarded as best representatives of the physical case studies typical of environmental and hydrodynamic applications described in Section 2. The solution procedure for each test case has been discussed in the previous section; numerical solution effects and other related issues such as convergence problems, advection and time-marching schemes, etc., can be found in the referenced papers.

4.1. Gas dispersion around an isolated building

This test case was studied experimentally and numerically by Delaunay et al. (1995) and Delaunay et al. (1997) at the CSTB of Nantes, France. Details of the experimental conditions can be found in Delaunay et al. (1995). The goal of the investigation was to understand the way external flow conditions may affect the dispersion of the contaminant around a building (isolated or placed within an aggregate of similar buildings). We report here on the results of a single building only. The 1/125 scale building model ($H^2 \times 6H$) was placed within an atmospheric wind tunnel having a working cross-section of 8 m^2. The incident wind impinging on the lateral face of the obstacle was highly turbulent ($T_u \approx 16\%$), and the Reynolds numbers based on the model height ranged between 10.000 and 40.000. A mixture of air and ethane was ejected at a speed of 2 m/s from six chimneys 4 mm in diameter and 96 mm high. The computational grid employed for high-*Re* computations consisted of 370.000 grid points, whereas the one used for computations with the two-layer k–ϵ model comprised 1.000000 nodes. In both cases the grid covered only half the domain. The calculation procedure was based on the Eulerian–Eulerian approach discussed previously. Turbulent stresses were modelled by means of two different eddy viscosity models and a second-moment closure.

The predicted flow fields in the vicinity of the obstacle clearly indicated that the various recirculations of the wind (on the sides and on top of the building) can be captured only with the SMC approach, despite the fact that the low-*Re* EVM computations provided a much better flow resolution near the ground wall (results not included here). An earlier result obtained with the standard model is shown in Fig. 1(a); it shows a rather complex flow structure with a large recirculation behind the obstacle and a horseshoe vortex close to the wall. However, a close look at the figure reveals that the k–ϵ model with wall functions produces an unrealistic re-attachment on the roof, whereas experimental observations have shown that the flow there separates from the leading edge and re-attaches at the trailing edge of the obstacle. Another computation has shown that using the two-layer approach alone will not prevent unrealistic re-attachment of the flow on the roof either. This behaviour is well recognized to be the direct consequence of employing EVMs, since these tend to produce spurious amounts of turbulent viscosity in the stagnation

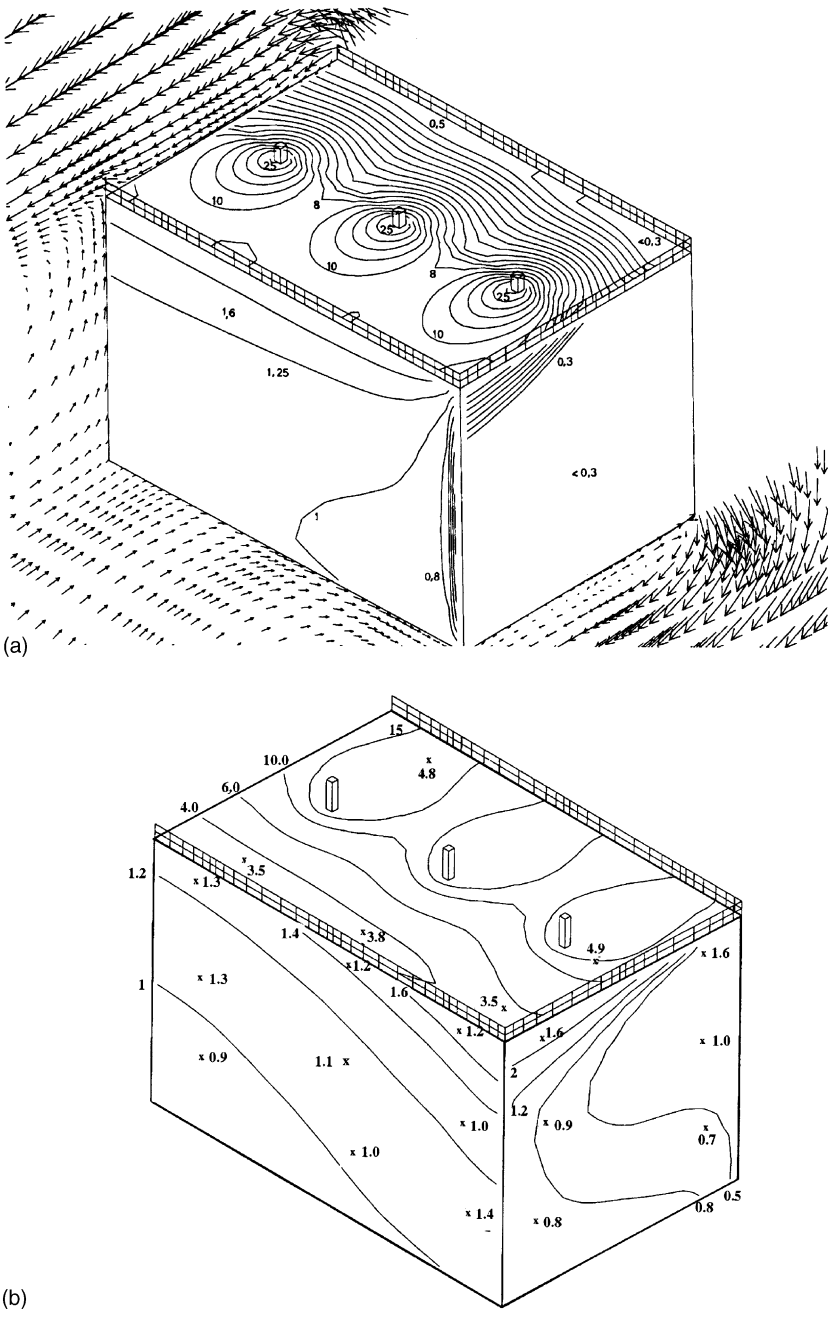

Fig. 1. Distribution of contaminant isocontours. (a) k–ϵ results (from Delaunay et al., 1995); (b) SMC results (from Delaunay et al., 1997); continuous lines: calculations, x symbols: experimental results.

region, altering the resolution on top of the obstacle (Lakehal and Rodi, 1997). Consequently the error in the concentration field calculated with EVMs may attain ≈100% (Fig. 1(a) does not include experimental results). In contrast, SMC results reported in Fig. 1(b) compare very well

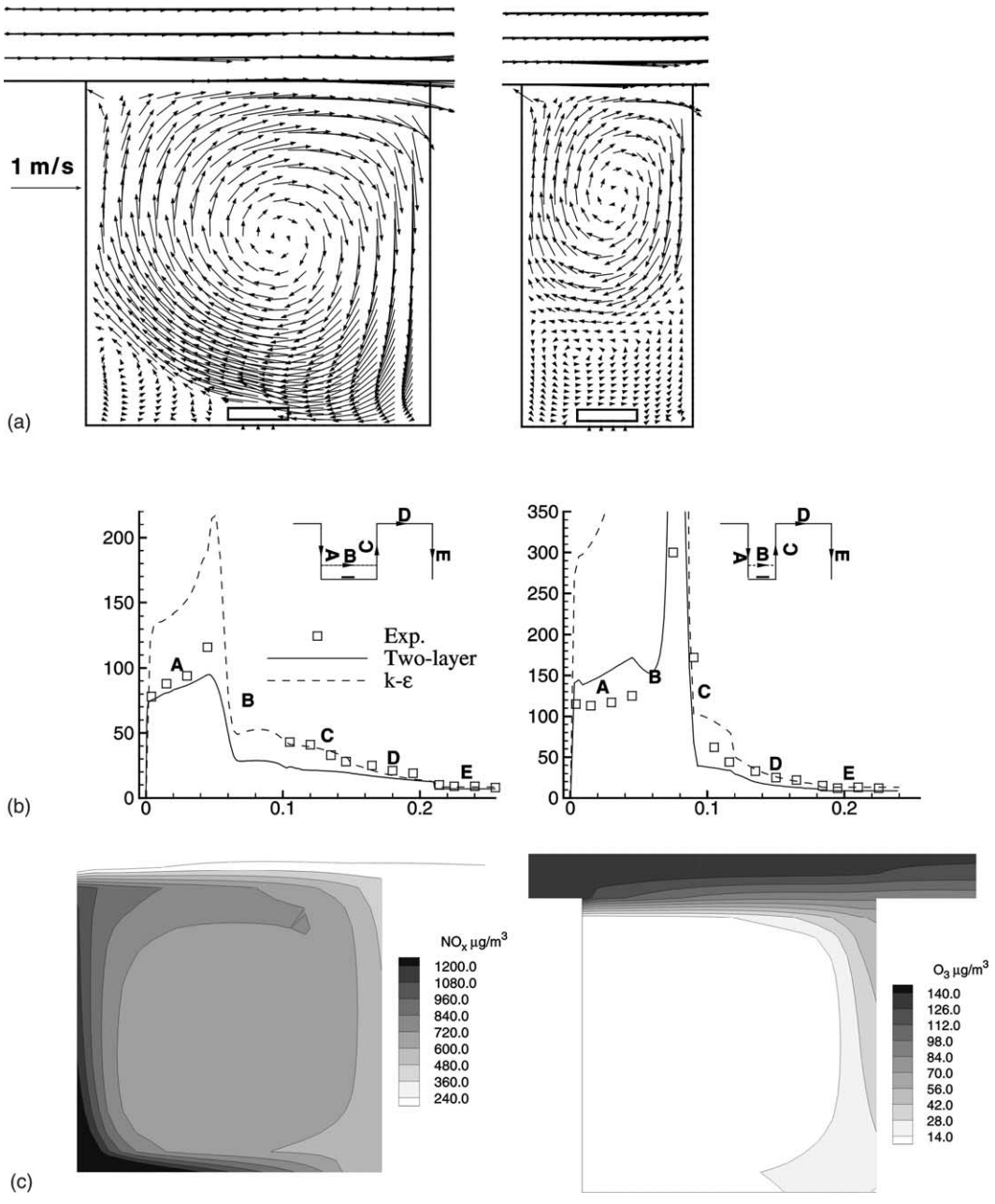

Fig. 2. Velocity vectors (a), non-dimensional concentrations (b), and pollutant concentrations NO_x – left and O_3 – right (c) computed with the k–ϵ model and the two-layer model for the square (left, a and b) and deep (right, a and b) flat-roof cases (from Theodoridis and Moussiopoulos, 2000).

with the data. Iso-contours of concentration on both the side and the leeward walls were predicted perfectly. The lack of measurements on top of the obstacle did not allow further comparison. Also, using the generalized gradient law GGDH for the scalar flux did not show any particular

advantage over the simplified gradient law. The conclusion of this investigation confirmed a statement postulated earlier: Second-moment closures are the minimum level of modelling required for turbulent mixing of a passive scalar in highly strained flows featuring a significant rate of turbulence anisotropy.

4.2. Pollutant dispersion within a street canyon

As mentioned previously, this case was investigated by Theodoridis and Moussiopoulos (2000) (see also Moussiopoulos et al., 1998). Two street canyon configurations were used, a rectangular one with a height-to-width ratio H/W equal to 1, and a deep one with $H/W = 2$. The conditions of a typical atmospheric boundary layer were set as inflow conditions based on the experiment reported by Rafailidis (2000).

Fig. 2(a) illustrates the velocity fields; it shows the development of a primary large-scale vortex covering most of the canyon region together with a smaller one at the leeward corner. In the deep-canyon configuration the corresponding primary vortex is much weaker, while almost stagnant conditions are established near street level due to the existence of a weak counter-rotating vortex. In Fig. 2(b), compares the distribution of the non-dimensional concentrations in both configurations. In the first case the maximum concentrations appear on the leeward wall due to the combined actions of the two vortices. The standard models tend to overestimate the peak concentration, but apart from this behaviour the results are globally satisfactory. The corresponding NO_x and O_3 concentration levels are displayed in Fig. 2(c): It shows high-NO_x concentration levels on the leeward side, while O_3 seems to be depleted within the canyon. More importantly, this simulation has clearly demonstrated two facts: (i) the oxidation of NO and NO_2 leads to a significant increase in NO_2 concentration and (ii) the NO_2-to-NO_x ratio varies linearly with the background ozone levels.

Compared to the previous example, here the standard k–ϵ model and its low-*Re* variant show a real potential for capturing the flow and pollutant concentration fields. The reason for this is attributable to the considerable complexity of the three-dimensional problem (CS1), which poses a great challenge to conventional eddy-viscosity models, known for their vulnerability to capture impinging flows followed by recirculations. The flow structure within the two-dimensional canyon is obviously less complex than that around the building. The present results suggest the standard model to be well suited for use with a Navier–Stokes solver as a fast and robust predictive tool for identifying urban areas in which peaks of ozone could occur.

4.3. Droplet dispersion over a marine boundary layer

This case refers to the two-dimensional simulation of the turbulent transport and evaporation of droplets ejected by bursting bubbles within various simulated air–sea stable, near-neutral, and unstable marine boundary layers (MBL) performed by Edson and Fairall (1994) and Edson et al. (1996). The aim was to validate an integrated Eulerian–Lagrangian algorithm by comparing its results with droplet dispersion measurements made during the CLUSE [9] campaign conducted at

[9] CLUSE: a French acronym translating the one-dimensional stationary boundary layer.

IMST, Luminy, France (Mestayer et al., 1990). The two-dimensional computational domain scales exactly with the wind tunnel at IMST, i.e. 50 m × 0.85 m plane section. Turbulence in the wind tunnel was isotropic and homogeneous. The flow, temperature and specific humidity fields were calculated according to the description given in Section 3.1.3, and reference was made to the k–ϵ model modified to account for buoyancy-induced production. The random-flight algorithm employed was based on formulation F1 described previously. More details on the computational methodology are available in Edson et al. (1996).

Flow field results due to the use of the Eulerian model in general compared very well with measurements. Note that this comparison was made first for an equilibrium channel flow; the marine boundary layer results were later compared with the Lagrangian results of the model. The same trend was also apparent in the vertical temperature and humidity profiles predicted at various locations and for three different humidity levels (95%, 77%, and 55%). Of primary interest among results of the Eulerian model is the shear stress $-\overline{u'w'}$ profile depicted in Fig. 3(left), which also compares well with the data at the wind speed of 7.5 m/s. This result confirms that the standard model is capable of simulating the two-dimensional developing surface layer with reasonable accuracy. The question on how the quality of these Eulerian results affect the output of the Lagrangian module is answered in the context of Fig. 3(right). The figure compares droplet volume spectra as functions of droplet radius and shows the Lagrangian part of the coupled algorithm to perform very well, too, except that it underestimates the vertical dispersion of larger droplets. This result may first suggest that random-flight schemes must use the same spatial dimensionality as the flow field. The influence of droplets on the scalar fields is discussed in the context of Fig. 4. The left part of the figure presents the difference in temperature profiles due to the presence of droplets. It shows that the near-surface air temperature increases with specific humidity, i.e. there is a release of sensible heat, which, according to the authors, is attributable to weak evaporative cooling at high humidity. The figure on the right side displays the change in the

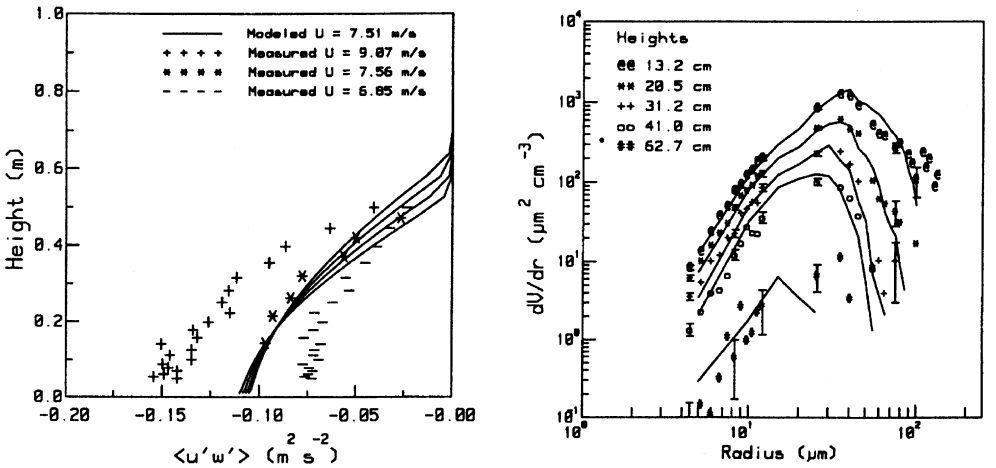

Fig. 3. Predicted $\overline{u'w'}$ profiles (left) and droplet volume spectra as a function of radius (right) versus experimental data taken at the CLUSE campaign – IMST, France. Results taken from Edson et al. (1996).

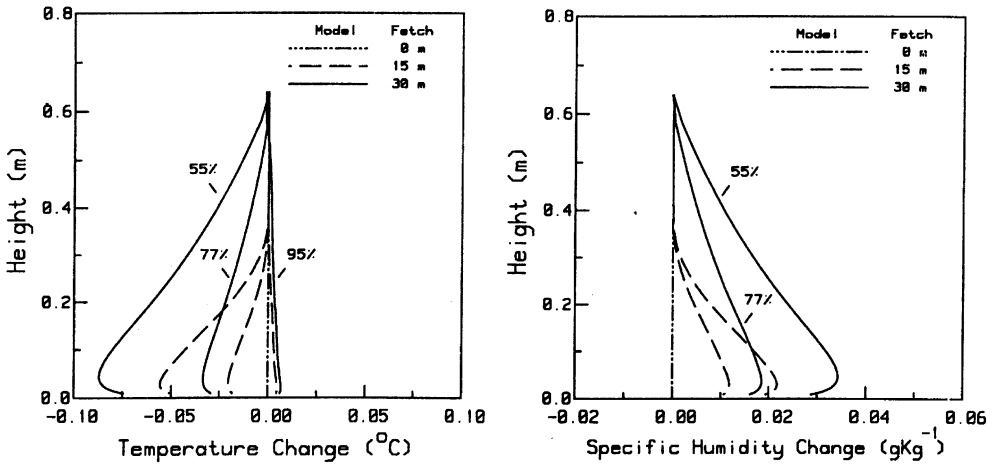

Fig. 4. Influence of droplet evaporation on the temperature field (left) and the specific humidity field (right). Results taken from Edson et al. (1996).

specific humidity field induced by the droplets. Physically, it conforms to the previous figure in that, due to the evaporation of droplets, the lower near-surface temperatures are associated with higher specific humidities.

Before proceeding further with the comparisons, it is worth examining the performance of formulation F1 in predicting the dispersion of both small and heavier droplets, i.e. 20 and 100 μm in diameter (Fig. 5), by way of an earlier investigation of the authors (Edson and Fairall, 1994). These results indicate a clear dispersion of the smallest droplets, whereas heavier ones are dominated by inertia. In a separate simulation reproducing droplet dispersion within a high-wind marine boundary layer, representative of conditions of an open ocean, the authors pointed out a significant influence of droplet evaporation on the surface energy budget, in particular both the mean profiles and the sensible and latent heat profiles may be strongly affected by the droplet ejection height (Edson et al., 1996).

This challenging test case reveals that a coupled Eulerian–Lagrangian model is capable of simulating the influence of droplet evaporation and sensible heat release on the surface energy budget. Among the various findings, the authors concluded that an increase in turbulence intensity due to high-shear rates does not increase the effect of droplet evaporation on the temperature and humidity fields as long as the waves do not participate in ejecting further droplets. Understandably, this issue to date still is an open question. In particular, the possible amplification of particle vertical dispersion by the waves has not yet been clarified. The random flight algorithm F1 employed for this case was developed for isotropic turbulence and accounts for particle dispersion in one direction only. The success of this investigation is related to the nature of the reproduced flow; indeed, a developing surface layer with an oncoming quasi-isotropic turbulence is conceptually in reach of a simple eddy-viscosity model. However, it is not yet clear whether the modifications to the surface energy budget are due to small droplets or to heavier ones. The answer to this question will indirectly help examine and evaluate the parametrization of the Lagrangian model assuming isotropic turbulence. In other words, it is possible that large

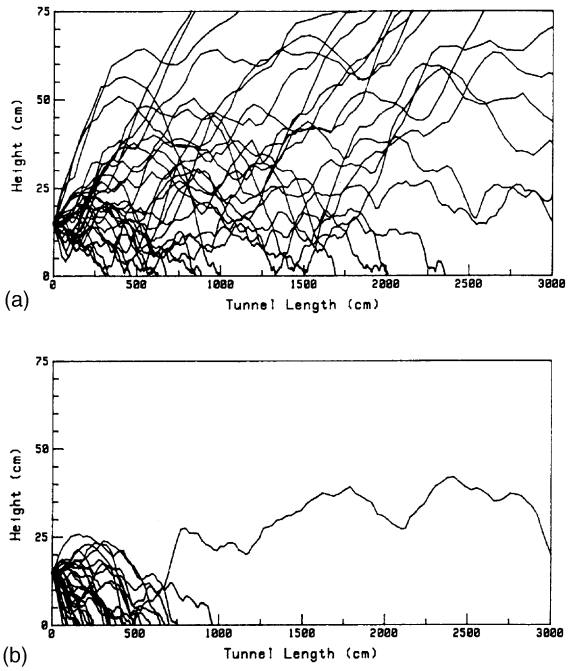

Fig. 5. Simulated droplet trajectories from the CLUSE campaign: (a) $D = 20$ μm and (b) $D = 100$ μm. Results taken from Edson and Fairall (1994).

droplets are the only source responsible for the distortion of the surface energy budget, in which case subjecting their motion to field turbulence is simply useless.

4.4. Tracking raindrops and impact in a street canyon

This test case was studied by Lakehal (1991) and Lakehal et al. (1995). It forms part of a more general investigation dealing with pollutant dispersion in the urban atmosphere (Mestayer et al., 1993). The flow field was computed in a two-dimensional plane and the effects of thermal stratification were ignored. The standard k–ϵ model was employed with wall functions. The structure of the flow inside the canyon obtained from the Eulerian part of the model (results not included here) is very similar to that shown in Fig. 2(a): the wind flow above the canyon is only slightly perturbed as is typical of "skimming flows" over relatively narrow streets, and a large-scale vortex structure is established within the canyon, close to the wind-facing wall.

In this simulation, the rain was simulated by a line of 100 elevated point sources located at an arbitrary height of three times the building height, each ejecting 200 particles of different diameters ($0.2 < D < 1$ mm). The initial particle velocity was set equal to its steady-state fall velocity. Fig. 6(a) displays particle trajectories of a series of five drops ($D = 0.2$ mm) ejected from selected point sources using formulation F1; a similar simulation with model F2 is displayed in Fig. 6(b). As compared to the simulations (results not shown here) with heavier droplets ($D = 1.0$ mm), the effects of turbulent dispersion were most noticeable for the smallest particles. In fact, the large

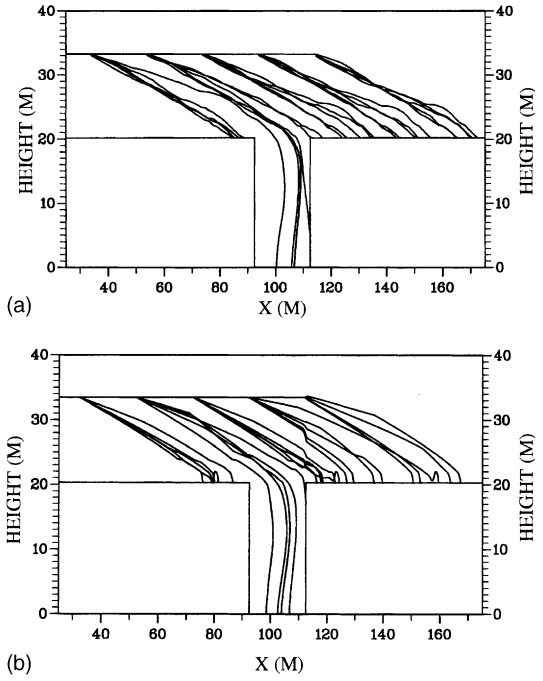

Fig. 6. Series of particle trajectories obtained using models F1 (a) and F2 (b) for particle diameter $D = 0.2$ mm, and (c) $D = 1$ mm using F1 (from Lakehal et al., 1995).

drops can only be slightly deviated by the mean motion of air and their vertical dispersion apparently remains negligible.

The raindrop spectrum in this simulation was based on the semi-empirical formulation of Best (1950). The Lagrangian module determines the trajectory of each particle until it impacts a surface. The water flow rate can then be collected per unit time and unit area over each surface, and the quantity effectively collected can be determined by combining those data with the rain spectrum of Best (1950). The experimental data employed for comparison originate from the field measurements of Hilaire and Savina (1989) at an outdoor site in Nantes, France. Fig. 7 compares the computed water rates, normalized to the number of injected drops in this category, with the numerical (dashed lines) and experimental (symbols) results of Hilaire and Savina (1989). Their measurements were made with driving rain collectors deployed at two levels (about 9 and 14 m) at the centre and close to both ends of the windward-facing walls of the first and third buildings in the array. The third building is referred to as the "protected building", and the first as the "unprotected building". While the measurements close to the building corners have been analyzed from a wind-engineering point of view, only the measurements made in the Euler–Lagrangian simulation of raindrop trajectories on the central section of the facades can be compared to the two-dimensional simulations. Hilaire and Savina (1989) simulations were based on the computation of mean flow lines for drops of various sizes, deducing the air mean flow lines from Wise (1965) flow measurements in a wind tunnel around one isolated and two parallel model buildings.

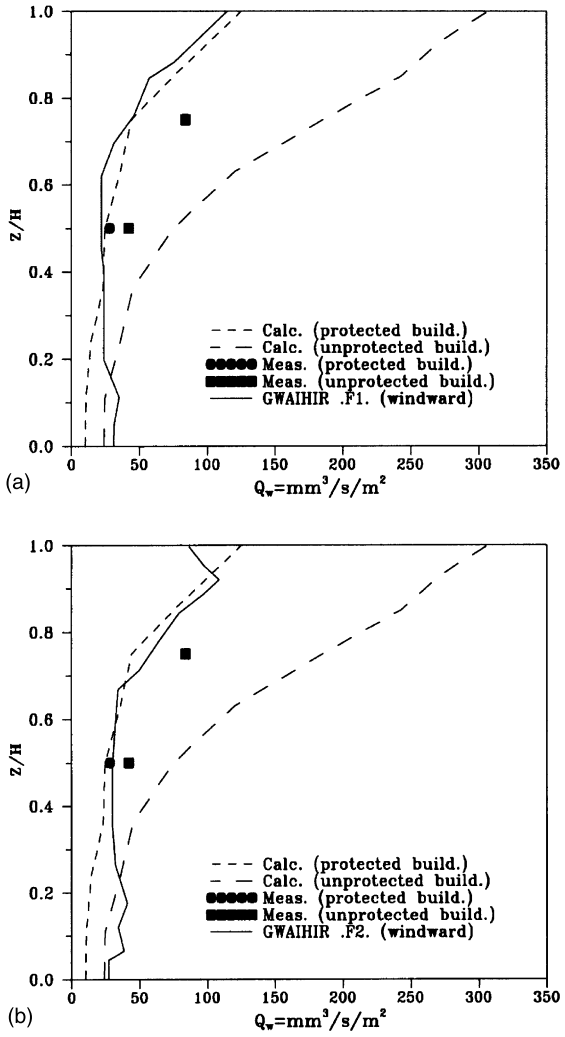

Fig. 7. Computed (Lakehal et al., 1995) vs. measured (Hilaire and Savina, 1989) total rates of water impinging on the windward wall of unprotected (a) and shadowed buildings (b).

Their calculations largely overestimate the measurements on the unprotected building. They agree relatively well with the measurements on the protected building and with the present simulations using models FI and F2. Although there exists only a small number of reliable measurements, the encouraging predictive performance of the different Lagrangian models applied in this case is noticeable. As was expected on the basis of results of the second computational example, the standard model is capable of predicting quite well the flow within the two-dimensional canyon.

In conclusion, proper modelling of this type of flow would require the inclusion of the dispersion in the direction normal to the mean particle trajectory (e.g. transition to formulation F3)

and the computation of all particle velocity components (e.g. Haworth and Pope, 1987). In strongly anisotropic turbulence the corrections enumerated previously for the correlation time scale and velocity sampling would be of little effect without a second-order closure model. The other alternative that needs to be explored is the one based on the LES of the flow field, providing the Eulerian turbulence statistics without approximation. In a first step these data can be employed to determine the particle turbulence statistics at the subgrid level following the same similarity principles as those given by Eqs. (24) and (25). This was already done by Wang and Squires (1996) who modelled the subgrid-scale (SGS) velocities as a random Gaussian process and added them to the filtered field. For the specific application they considered (aerosol dispersion) the effect of the SGS model on the particle motion was negligible. The same conclusion was drawn by Armenio et al. (1999), who explored the effect of the SGSs on IP motion, and it is most likely that heavier particles will be even less sensitive to SGS turbulence and will not require SGS modelling either.

4.5. Sedimentation in an axisymmetric circular tank

Flows similar to the one presented below (due to Lakehal et al., 1999) including strong density effects, were already reported by Lyn et al. (1992), Zhou et al. (1992), Zhou and McCorquodale (1992), Szalai et al. (1994), Krebs et al. (1996) and others. Most of these contributions applied the k–ϵ turbulence model in two dimensions, except for Vitasovic et al. (1997) who extended the calculations to three dimensions. However, Zhou and McCorquodale (1992) employed an algebraic stress model and this results in better predictions than the standard model. Compared to these and to many other studies the contribution of Lakehal et al. (1999) to be discussed here introduced further innovations with the inclusion of a rheology function to the highly concentrated sludge mixtures. Their approach was somewhat different from that of Dahl et al. (1994). It should be emphasized that at the time these simulations were conducted no reliable measurements were available to verify the results produced by the numerical method.

The flow field was obtained by solving the unsteady axisymmetric RANS equations in a cylindrical coordinate system. The k–ϵ model was used for turbulence modelling, together with wall functions. The suspended sediment concentration was determined by solving Eq. (3), into which the particle settling velocity was introduced. Also, the damping influence of stratification on the production of turbulent kinetic energy was expressed as a source term appearing in the transport equations of turbulent kinetic energy k and its rate of dissipation.

The computational domain is shown in Fig. 8(a). The panels below present snapshots of the concentration field predicted at three time steps in the situation referred to by the authors as *the reference case*, i.e. the constant C_3 in Eq. (13) was set equal to unity. These snapshots reveal in particular the best known features of this flow, such as a quasi-coherent large-scale motion about the interface, an induced reverse flow on top of the sludge, a forward-flow layer developing on top of the reverse flow and below it, a counter current causing the part of the sludge blanket near the bottom to flow towards the central sludge withdrawal, etc. (cf. van Marle and Kranenburg, 1994; Krebs et al., 1996). The sensitivity to the value of C_3 is analyzed in the context of Figs. 9(a) and (b), displaying the velocity and concentration profiles resulting from calculations with variable C_3-values. Including the sink term P_B in Eq. (13) causes the values of turbulence dissipation rate ε to decrease and subsequently those of the eddy viscosity ν_t to increase. An increasing ν_t in turn

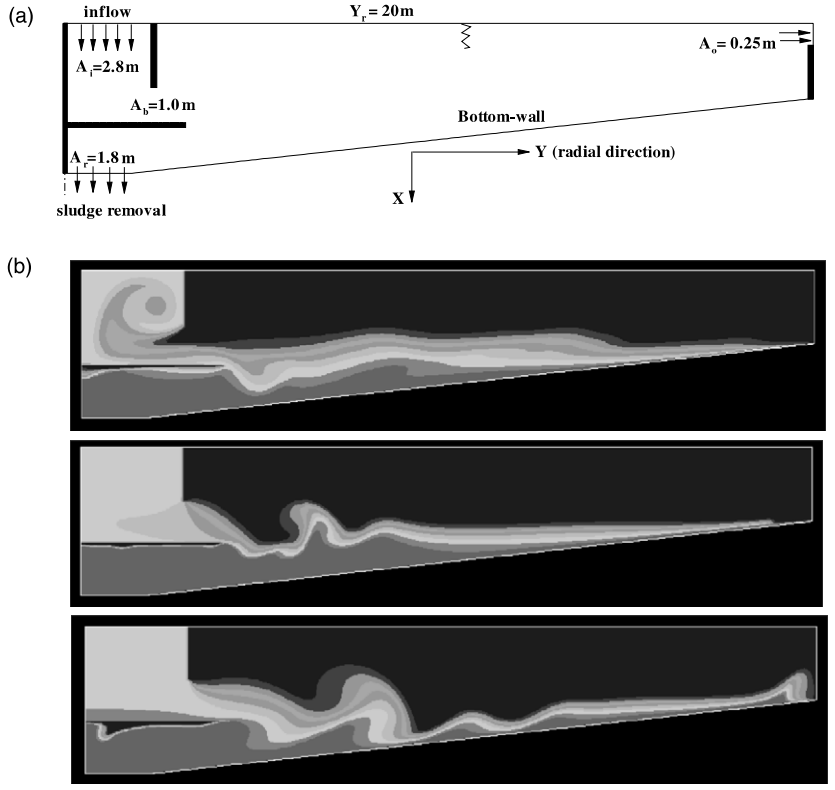

Fig. 8. Computational domain (a) and time evolution of scalar concentration at three time-steps (b) during the early stage of the simulation.

promotes the turbulent diffusive transport of all quantities. Since the strongest influence of this kind is obtained with $C_3 = 0$, the velocity and concentration gradients are smoothed with distance from the inlet, while without sink term in Eq. (13), $C_3 = 1.0$, gradients remain much sharper throughout the tank; the sludge blanket remains more compact and better defined. This behaviour reveals the crucial importance of determining the eddy viscosity in the computation of buoyancy-affected flow and hindered settling of activated sludge. In conclusion, this shows the need for reliable experimental investigations for the purpose of model calibration and verification, especially for distinctly stratified flow.

The influence of the Bingham rheology approach, Eq. (9), on the flow and concentration profiles is shown in Figs. 10(a) and (b). Generally introducing a plastic viscosity μ_p as a function of concentration and a yield stress τ_b causes the sludge blanket to rise while its surface remains sharp; see Fig. 10(b). But as shown in Fig. 10(a), the velocities within the sludge blanket decrease as the applied shear stress now produces a smaller shear rate. The role played by the yield stress is made more apparent by drastically increasing the value of τ_b by a factor of 100 in order to consider the stiffness of the sludge under small shear and high-concentration conditions. The analysis of rheology effects gives a clear indication of the sludge removal mechanism. Since in prototypes the settled sludge cannot be removed without removal equipment, while the numerical model suggests

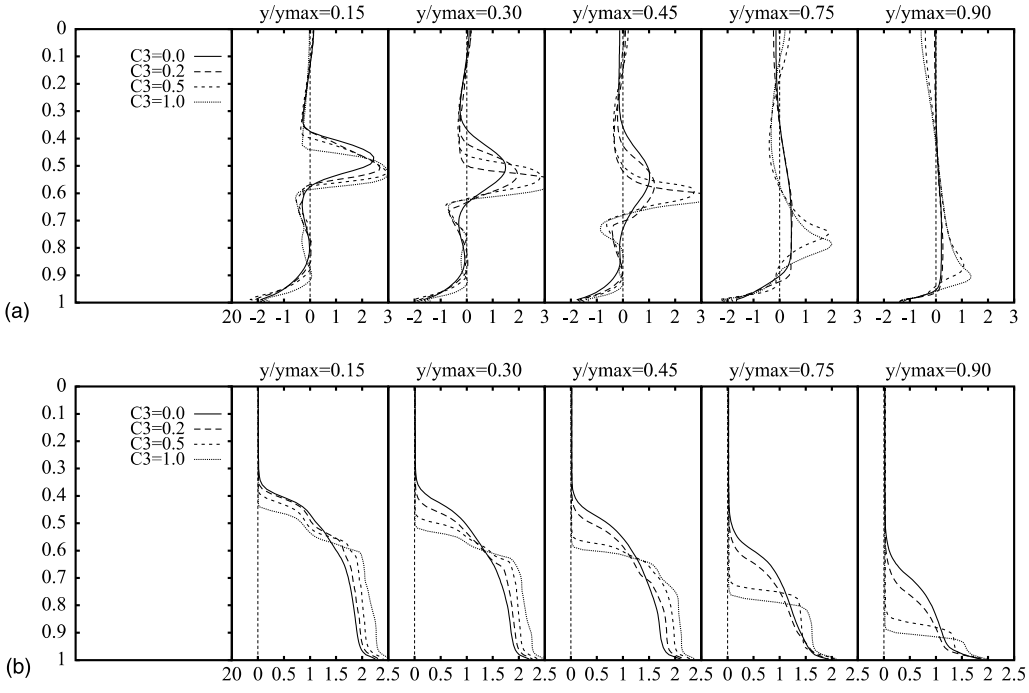

Fig. 9. Influence of turbulence-model constants C_3 on the radial velocity (a) and particle concentration (b). Results taken from Lakehal et al. (1999).

a self-sustaining sludge transport, the thickened sludge must in fact exhibit a distinct Bingham-type behaviour. Lakehal et al. (1999) and later Armbruster et al. (2001) concluded that in a tank with inclined bottom the function of a scraper removal system is to overcome the yield stress and to make the mixture flow rather than to induce a centerward sludge transport as such. Apart from this, the authors of that work also investigated the effect of varying the settling velocity function (Eq. (8)). With an alternative set of parameters typical for another design they observed a strong influence on the thickening characteristics of the sludge, similar to what has been observed with varying coefficient C_3 in Eq. (13).

To summarize, this application highlights two major uncertainties: Both the constitutive equations for the dispersed phase and the settling velocity function are directly based on experimental data. But more importantly, this class of flow cannot be treated with a turbulence model offering a large flexibility for tuning constants, in particular those associated with buoyancy-driven forces.

4.6. Analysis of a confined bubble plume

In most of the experiments dealing with air-bubble plumes water has always been utilized as simulant material, though some work on helium–water and nitrogen–mercury systems has also been reported; see, for example, Mazumdar and Guthrie (1995) for a review. The data refer exclusively to the injection of non-condensible gases into liquid pools. The main experimental

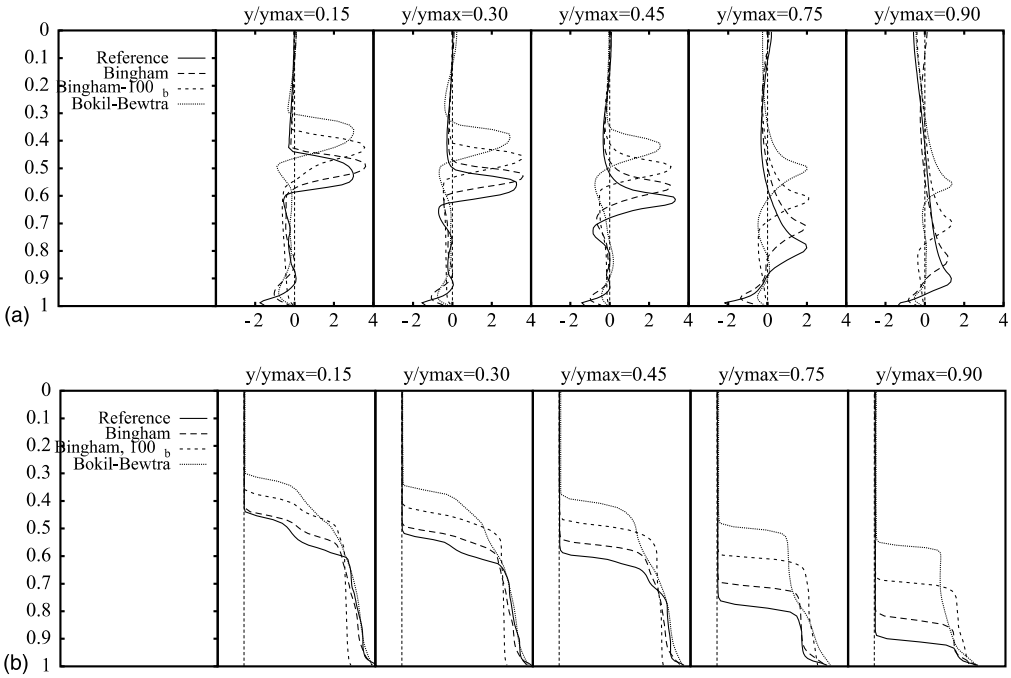

Fig. 10. Effect of the Bingham plastic model on the radial velocity (a) and particle concentration (b). Results taken from Lakehal et al. (1999).

findings can be summarized as follows: For air-water systems, bubble spreading is approximately linear, whereas for helium-water and nitrogen-mercury systems the lateral plume growth can be more pronounced. In all cases the radial distribution of void fraction α, bubble frequency, and gas and liquid rise velocities follow a Gaussian distribution. Also, an unsteady distortion of the plume may occur, although at a non-regular frequency. It is of course expected that by use of rigorous computational methods for this type of flow, together with appropriate modelling strategies for the physical mechanisms could lead to a reasonable prediction of these general trends.

The present results are taken from a validation exercise based on air-water tests reported by Anagbo and Brimacombe (1990), in which a clear bubble swarm was produced by air injection into a cylindrical water vessel through a porous plug in its base. The bubble plume rises to the surface, entraining liquid from the pool and generating a large-scale circulation. The results presented here were obtained by Smith and Milelli (1998) from their analysis of the case of the lowest gas-injection-rate ($\mathscr{M} = 12$ l/min.); in the experiment this particular flow condition led to negligible fragmentation and coalescence and to a uniform bubble size-distribution ($D \approx 3$ mm) with height. At the inflow plane, the gas velocity was adjusted to reproduce the total gas flow rate $\mathscr{M}$ with the liquid and gas volume fractions set equal to $\alpha^{l} = 0.38$, $\alpha^{g} = 0.62$, and axial velocities $\overline{W_l} = 0.0$ m/s and $\overline{W_g} = 0.114$ m/s, respectively. More details on the solution procedure and boundary conditions can be found in the cited paper.

Computed plume widths at three elevations are compared against (normalized) experimental data in Table 1 for each model. Some of the rows in the table are grouped into pairs to indicate

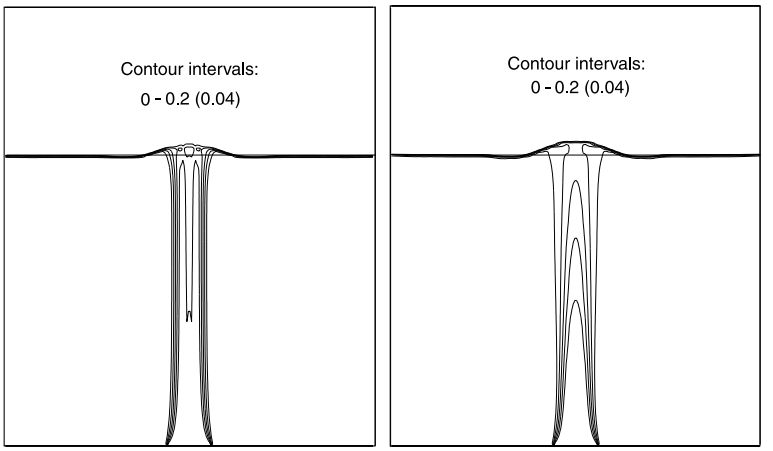

Fig. 11. Void fraction distributions in the midplane of the pool: (left) without turbulent dispersion model; (right) with the TDF model. Results taken from Smith and Milelli (1998).

analogous modelling assumptions. The RDM of Smith and Milelli (1998) for bubble–eddy interaction (see Section 3.1.2) introduces artificial variations in the scale of the eddy lifetimes ($\tau_e \sim 0.2$–$0.3s$), in very much the same as by use of Eq. (27) for the class of random flight algorithm discussed in Section 3.4.4. These imposed changes in time scales will be superimposed on those of the mean flow. A meaningful comparison of results with the *turbulent dispersion force* (generally employed in steady state) model can therefore be obtained only after averaging.

For the reference case, Case 1, with no forces apart from buoyancy and drag, no spreading of the plume occurs. This is clearly supported in the context of Fig. 11(left) displaying the void fraction contours in a vertical plane through the centre of the plug. Cases 2 and 3 confirm that the (empirical) TDF and (mechanistic) RDM models both induce plume spreading by identical amounts; see Table 1. The contour plot in Fig. 11(right) shows that some spreading has actually occurred using the TDF model, but the spreading angle remains relatively small ($\sim 5°$). The remaining rows in Table 1 demonstrate that the TDF model is very sensitive to further modelling assumptions, and it is therefore possible to optimize coefficients in order to obtain a better fit to experimental data. Radial profiles of the bubble and liquid rise velocities 30 cm above the plug for both models (cases 7/8 in Table 1) are shown in Fig. 12. Those of the RDM model are long-term averages. None of the models is capable of correctly reproducing the center-line bubble velocity, and, even though predicted results for the liquid velocity follow the experiments, the overall values are predicted too low. In summary, the RDM model seems to be much more resilient, and its strictly mechanistic approach to turbulent dispersion would seem to offer better opportunities for the development of trustworthy, two-phase-flow turbulence models. This rationale should underline an increasing interest in LES approaches for the prediction of this class of flow, but since this is a new territory, various roadblocks need to be circumvented first, as will be discussed in the concluding section below. Note, though, that the authors from whom these numerical results were borrowed are already exploring the LES approach for this class of flow (Milelli et al., 2002a,b).

Table 1
Comparison of plume spreading statistics for various model assumptions

Case no.	Model identifier	Elevation (mm)		
		100	200	300
0	Experiment	100	100	100
1	No Models	73	48	36
2	TDF	75	68	72
3	RDM	75	68	69
4	TDF+SV	100	100	95
5	RDM+SV	80	75	69
6	TDF+SV+L(0.5)	118	117	113
7	RDM+SV+L(0.5)	91	80	79
8	TDF+SV+L(0.1)	100	100	90
9	RDM+SV+L(0.1)	74	63	63

TDF—Turbulent Dispersion Force, RDM—Random Dispersion Model, L—Lift force (with coeff.) SV—Simonin and Viollet Model.

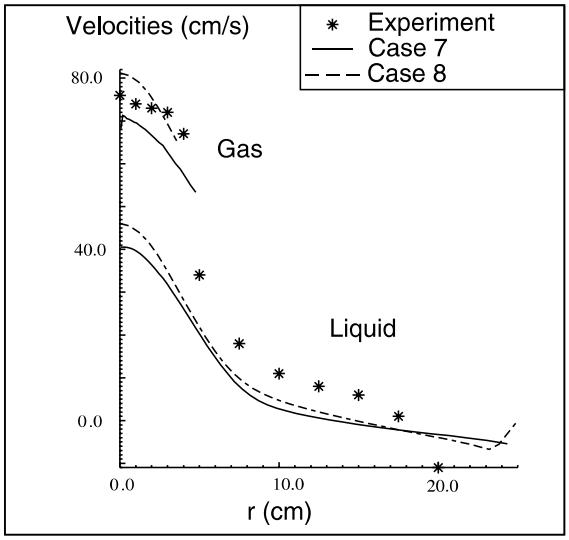

Fig. 12. Mean bubble and liquid rise velocities obtained with both approaches for modelling the TDF. Results taken from Smith and Milelli (1998).

5. Concluding remarks and future developments

In this paper selected applications typical in environmental and hydrodynamic research were introduced together with the corresponding solution procedures adopted over the past nearly three decades, some of which have occasionally been of debatable quality. The aim of the contribution was to highlight the progress achieved in simulating these flows, with an emphasis on the

efficiency of computational analyses in general and their actual role in prediction and design processes. The deliberate choice of these applications was motivated by the variety of their properties: Flows were either isothermal or stratified, with or without phase change, with both Newtonian and non-Newtonian properties, etc. The dispersed phases were of different kind, too: Particles, droplets, bubbles, almost passive or with settling properties, smaller than the Kolmogorov micro-scale and heavier than the carrier fluid, etc. Even if the paper is not written in the strict spirit of a review, the introduction of various applications together with the solution methods may serve as a guideline for newcomers to this wide field since it attempts to indicate which solution method is to be employed for a particular type of problem.

The central remarks to be emphasized on the basis of the case studies presented here are:

- The error in the dispersed concentration field around blunt structures may attain ≈100% when resorting to EVMs. Low-*Re* variants are not capable of performing any better; they are not suitable for atmospheric type flows anyway. The presented results have been confirmed in other works dealing with gas releases from groups of buildings, e.g. Hangan (1999) and Castro et al. (1999); the latter contribution reports on deviations of EVMs predictions from measurements of about ≈50%. Reynolds stress models were found to be the minimum level of closure required for the mixing of contaminants around a single obstacle, where turbulence is highly anisotropic. But if this sophisticated strategy has proven valuable in view of the example presented, this does not mean that it would perform with comparable accuracy for a typical urban canopy, where the flow is very complex. Recent LES applications to similar flows, e.g. Rodi et al. (1997), have shown a clear superiority over RANS simulations. The interest in LES for the prediction of atmospheric dispersion in general is now gaining in popularity, and promising results have already been communicated, e.g. by Patton et al. (1998) and Murakami (1997).
- In the sedimentation problem, turbulence equations were found to lack correct parametrization and a strong dependence of results on the value of a single constant associated with the buoyancy generation term was revealed. And, although these buoyancy forces were found to dominate over turbulent stresses, a complete SMC for all turbulent fluxes appears to be necessary, along with a prognostic equation for the scalar variance $\overline{c'^2}$. Another plausible alternative would consist in employing an algebraic k–$\overline{c'^2}$–ε–ε_c model as proposed by Kenjeres and Hanjalic (2000), in which the turbulent scalar flux $\overline{u'_j c'}$ is provided by an algebraic flux model. The advantage of using this form is that it includes all terms responsible for the production, i.e. by scalar gradients, mechanical deformation, and buoyancy-driven turbulence modulation. Extra transport equations for the scalar variance and its rate of dissipation ε_c are necessary, though. Apart from the turbulence modelling issue, the investigation revealed the importance of appropriate parametrization of the settling velocity and the constitutive equations for the non-Newtonian material. But, unlike for turbulence modelling, there is not much to expect apart from referring to reliable experiments.
- Results of modelling the dispersion of evaporative droplets over the marine boundary layer using the random-walk model F1 compared well with measurements. This is partially due to the favorable experimental conditions that have been reproduced by the model: An isotropic grid turbulence in a quasi-homogeneous flow. The relevant processes representing the conditions over the oceans are not easy to reproduce; the model may then behave differently. In the other

example involving raindrop tracking, the random flight models for heavy particles with inertia were almost of equal predictive performance, although those based on the Langevin equation were slightly better in sensitizing the smallest particle trajectories to the field turbulence. All variants have readily shown that turbulent dispersion is most noticeable for the smallest particles only ($D < 0.5$ mm). Apart from this, coupling these Lagrangian techniques with isotropic turbulence models has been and will remain questionable. First difficulties already appeared with the case of impacting rain drops, as compared to the dispersion of droplets over the marine boundary layer, and it is likely that further difficulties will be faced in more challenging complex flows. The main weakness of Markov chain approaches based on the Langevin equation (written in the forms discussed in this paper) is their construction on the basis of a single particle velocity fluctuation. MacInnes and Bracco (1992) proved that even under its simplified variant, the generalized Langevin equation of Haworth and Pope (1987) (not discussed in the corresponding section) which involves the generation of the three-dimensional fluctuating field is the best in its class. Several important modifications to the other type models based on the random generation of eddies were discussed in this paper, too, but it is evident that only with the LES approach can the number of approximations be substantially reduced.

- The hypothesis of turbulence isotropy is known to be notoriously incorrect in case of bubble plumes. The Reynolds stress models, which in principle are appropriate for anisotropic turbulent flows, are unstable and not sufficiently robust. But even with the help of this strategy it is most likely that the interaction between the large-scale structures and the bubbles will remain a matter of ad hoc approximation based on scaling arguments as long as Reynolds averaging is adopted. Therefore, attention must focus on LES in which the integral scales of turbulence are solved explicitly while only the SGS portion is modelled. The advantage in relation to bubble-laden flows is that the dispersed phase should directly (without model) interact with eddies having at least the same size, but not with the smallest ones. However, since this is a new field of study, many open questions will need to be addressed, in particular the way a universally accepted, two-phase SGS model including bubble-induced dissipation (if and when appropriate) can be derived.
- Apart from the optimization of settling tanks, turning to computational analyses of either type does not seem yet to contribute much to the prediction of pollutant and hydrometeor dispersion in the atmosphere. Paradoxally, the simulation of bubbly plumes seems to me much throughly investigated in metallurgy and nuclear energy research than in environmental hydrodynamics. Studying the dispersion of marine droplets and its global effect on the sea–air interaction remains confined to laboratory scales.

The central remarks enumerated above suggest that future developments should account for turbulence in a more sophisticated fashion. Indeed, apart from the case of particle sedimentation in water clarifiers, the other applications around which this work has been centered raise all the difficult challenges of considering the entire spectrum of scales ranging from those of micro droplets to those of large turbulent eddies evolving within the atmospheric boundary layer. Without any doubts, in this class of flow great interest in the near future will turn towards the LES approach. While examples like case studies CS1 and CS2 will not face particular difficulties, those treated within the Eulerian–Lagrangian framework would require new developments for particle turbulent statistics at the SGS level.

Acknowledgements

The author wishes to acknowledge the cooperation of Drs. P.G. Mestayer, S. Anquetin, J. Edson, D. Delaunay, G. Theodoridis, B.L. Smith, M. Milelli, Prof. P. Krebs, and Prof. W. Rodi, who permitted the use of their results. Thanks also go to Prof. G. Yadigaroglu and Ch. Narayanan for their valuable comments on this paper. Some of the presented calculations were performed while the author was affiliated with ECN and CSTB at Nantes in France and the University of Karlsruhe in Germany.

References

Ahmed, A.M., Elghobashi, S., 2000. On the mechanisms of modifying the structure of turbulent homogeneous shear flows by dispersed particles. Phys. Fluids 12, 2906–2930.

Anagbo, P.E., Brimacombe, J.K., 1990. Plume characteristics and liquid circulation in gas injection through a porous plug. Metall. Trans. B 21, 637–647.

Armbruster, M., Krebs, P., Rodi, W., 2001. Numerical modelling of dynamic sludge blanket behaviour in secondary clarifiers. Water Sci. Technol. 43, 173–180.

Armenio, V., Piomelli, U., Fiorotto, V., 1999. Effect of the subgrid scales on particle motion. Phys. Fluids 11, 3030–3041.

Beguin, D., 1985. Etude pour la France du risque de mouillage par la pluie des parois verticales de la construction. Report No. EN-CLI 85-82, CSTB Nantes, France.

Besnard, D.C., Harlow, F.H., 1988. Turbulence in multiphase flow. Int. J. Multiphase Flow 14, 679–699.

Best, A.C., 1950. The size distribution of raindrops. Q. J. R. Met. Soc. 76, 16–36.

Boivin, M., Simonin, O., Squires, K., 2000. On the prediction of gas–solid flows with two-way coupling using large eddy simulation. Phys. Fluids 12, 2080–2090.

Burk, S.D., 1984. The generation, turbulent transfer and deposition of the sea salt aerosol. J. Atmos. Sci. 41, 3040–3051.

Castro, I.P., Cowan, I.R., Robins, A.G., 1999. Simulation of flows around buildings. J. Aerospace Eng. 12, 145–160.

Carrica, P.M., Drew, D., Bonetto, F., Lahey, R.T., 1999. A polydisperse model for bubbly two-phase flow around surface ships. Int. J. Multiphase Flow 25, 257–305.

Chen, X., 2000. Heavy particles dispersion in inhomogeneous, anisotropic, turbulent flows. Int. J. Multiphase Flow 26, 635–661.

Choi, E.C.C., 1994. Determination of wind-driven-rain intensity on building faces. J. Wind Eng. Ind. Aerod. 51, 55–69.

Clift, R., Grace, J.R., Weber, M.E., 1978. Bubbles, Drops and Particles. Academic Press, New York.

Cowan, I.R., Castro, I.P, Robins, A.G., 1997. Numerical considerations for simulation of flow and dispersion around buildings. J. Wind Eng. Ind. Aerod. 67/68, 535–545.

Crowe, C.T., Trout, T.R., Chung, J.N., 1996. Numerical models for two-phase flows. Ann. Rev. Fluid. Mech. 28, 11–43.

Csanady, C., T, 1963. Turbulent diffusion of heavy particles in the atmosphere. J. Atmos. Sci. 20, 201–208.

Dahl, C.P., Larsen, T., Petersen, O., 1994. Numerical modelling and measurement in a test secondary settling tank. Water Sci. Technol. 30, 219–228.

Daly, B.J., Harlow, F.H., 1970. Transport equations in turbulence. Phys. Fluids A 13, 2634–2649.

Davidson, M.R., 1990. Numerical calculations of two-phase flow in a liquid bath with bottom gas injection: the central plume. Appl. Math. Modelling 14, 67–76.

De Baas, A.F., Van Dop, H., Nieuwstadt, F.T.M., 1986. An application of the Langevin equation for inhomogeneous conditions to dispersion in a convective boundary layer. Q. J. R. Met. Soc. 112, 165–180.

Delaunay, D., Lakehal, D., Grillaud, G., Barré, C., 1995. Analyse Quantitative de la Pollution de L'air Neuf Hygiénique par L'air Extrait des Batiments Résidentiels ou Tertiaires. Report EN-CLI 93.15C, CSTB Nantes, France.

Delaunay, D., Lakehal, D., Barré, C., Sacré, C., 1997. Numerical and wind-tunnel simulation of gas dispersion around a rectangular building. J. Wind Eng. Ind. Aerod. 67/68, 721–732.
Dick, R.I., Ewing, B., 1967. The rheology of activated sludge. J. Water Pollut. Control Federation 39, 543–560.
Drew, D.A., Lahey, R.T., 1987. The virtual mass and lift force on a sphere in rotating and straining inviscid flow. Int. J. Multiphase Flow 13, 113–121.
Drew, D.A., Passman, S.L., 1999. Theory of Multicomponent Fluids. Appl. Math. Sci., vol. 135. Springer-Verlag, New York.
Durbin, P.A., 1980. A random flight model of inhomogeneous turbulent dispersion. Phys. Fluids 23, 2151–2153.
Durst, F., Milojevic, D., Schonung, B., 1994. Eulerian and Lagrangian predictions of particulate two-phase flows: a numerical study. Appl. Math. Modelling 8, 101–115.
Edson, J.B., 1989. Lagrangian model simulation of the turbulent transport of evaporating jet droplets. Ph.D. Thesis, The Pennsylvania State University.
Edson, J.B., Fairall, C.W., 1994. Spray droplet modeling, 1. Lagrangian model simulation of the turbulent transport of evaporating droplets. J. Geophys. Res. 12, 25295–25311.
Edson, J.B., Anquetin, S., Mestayer, P.G., Sini, J.F., 1996. Spray droplet modeling, 2. An interactive Eulerian–Lagrangian model of evaporating spray droplets. J. Geophys. Res. 101, 1271–1293.
Elghobashi, S.E., Abou-Arab, T.W., 1982. A two-equation turbulence model for two-phase flows. Phys. Fluids 26, 931–937.
Elghobashi, S., 1994. On predicting particle-laden flows. Appl. Sci. Res. 52, 309–329.
Fairall, C.W., Hare, J.E., Edson, J.B., McGillis, W., 2000. Parametrization and micrometeorological measurement of air–sea gas transfer. Boundary-Layer Meteorol. 96, 63–106.
Gibson, M.M., Launder, B.E., 1978. The effects on pressure fluctuations in the atmospheric boundary layer. J. Fluid Mech. 86, 491–511.
Glendening, J.W., Burk, S.D., 1992. Turbulent transport from an arctic lead – a large-eddy simulation. Boundary-Layer Meteorol. 59, 315–339.
Gossman, A.D., Ioannides, E., 1981. Aspects of computer simulation of liquid-fuelled combustors. AIAA Paper 81-0323.
Graham, D.I., 1998. Improved eddy interaction models with random length and time scales. Int. J. Multiphase Flow 24, 335–345.
Gunn, R., Kinzer, G.D., 1949. The terminal velocity of fall for water droplets in stagnant air. J. Meteorol. 6, 243–248.
Hall, C.D., 1975. The simulation of particle motion in the atmosphere by a numerical random-walk model. Q. J. R. Met. Soc. 101, 235–244.
Hangan, H., 1999. Experimental numerical and analytical models for a dispersion study. J. Aerospace Eng. 12, 161–167.
Hilaire, J., Savina, H., 1989. Pluie battante sur une facade d'immeuble. Report No. EN-CLI 88.5 R, CSTB Nantes, France.
Hinze, J.0., 1975. Turbulence. McGraw-Hill, New York.
Haworth, D.C., Pope, S.B., 1987. A PDF modeling study of self-similar turbulent free shear flows. Phys. Fluids 30, 1026–1044.
Högström, U., 1996. Review of some basic characteristics of the atmospheric surface layer. Boundary-Layer Meteorol. 78, 215–246.
Ishii, M., 1975. Thermo-Fluid Dynamics Theory of Two-Phase Flow. Eyrolles, Paris.
Jin, Y., Guo, Q., Viraraghavan, T., 2000. Modeling of class I settling tanks. J. Environ. Eng. 126, 754–760.
Joseph, D.D., Lundgren, T.S., Jackson, R., Saville, D.A., 1990. Ensemble averaged and mixture theory equations for incompressible fluid–particle suspensions. Int. J. Multiphase Flow 16, 35–42.
Karagiozis, A., Hadjisophocleous, G., Cao, S., 1997. Wind-driven rain distributions on two buildings. J. Wind Eng. Ind. Aerod. 67/68, 559–572.
Karl, J.R., Wells, S.A., 1999. Numerical model of sedimentation/thickening with inertial effects. J. Environ. Eng. 125, 792–806.
Kastner-Klein, P., Federovich, E., Plate, E.J., 1997. Gaseous pollutant dispersion around urban-canopy element: wind tunnel case studies. Int. J. Environ. Pollut. 8, 727–737.

Kenjeres, S., Hanjalic, K., 2000. Convective rolls and heat transfer in finite-length Rayleigh–Benard convection: a two-dimensional numerical study. Phys. Rev. 62, 7987–7998.
Krebs, P., Stamou, A.I., García-Heras, J.L., Rodi, W., 1996. Influence of inlet and outlet configuration on the flow in secondary clarifiers. Water Sci. Technol. 34, 1–9.
Lacy, R.E., 1977. Climate and building in Britain. Building Research Establishment Report.
Lahey, R.T., Drew, D.A., 1988. The three-dimensional time and volume averaged conservation equations of two-phase flow. Adv. Nucl. Sci. Technol. 20, 1–69.
Lahey, R.T., Drew, D.A., 2001. The analysis of two-phase flow and heat transfer using a multidimensional, four field, two-fluid model. Nucl. Eng. Des. 204, 29–44.
Lakehal, D., 1991. Modélisation Lagrangienne des Hydrométéores dans la Canopée Urbaine. DEA Thesis, Ecole Centrale de Nantes, France.
Lakehal, D., Mestayer, P.G., Edson, J.B., Anquentin, S., Sini, J.F., 1995. Eulero–Lagrangian simulation of atmospheric rain drop trajectories and impacts inside the urban canopy. J. Atmos. Environ. B 29, 3501–3518.
Lakehal, D., Rodi, W., 1997. Calculation of the flow past a surface-mounted cube with two-layer turbulence models. J. Wind Eng. Ind. Aerod. 67/68, 65–78.
Lakehal, D., Krebs, P., Krijgsman, J., Rodi, W., 1999. Computing shear flows and sludge blanket in secondary clarifiers. ASCE J. Hydraul. Eng. 125, 253–262.
Lance, M., Bataille, J., 1991. Turbulence in the liquid phase of a uniform bubbly air–water flow. J. Fluids Mech. 222, 95–118.
Launder, B.E., Spalding, D.B., 1974. The numerical computation of turbulent flows. Comput. Meth. Appl. Mech. Eng. 3, 269–289.
Launder, B.E., Reece, G., Rodi, W., 1976. Progress in the development of a Reynolds stress turbulence closure. J. Fluid Mech. 68, 537–566.
Legg, B.J., 1983. Turbulent dispersion from an elevated line source: Markov chain simulations of concentrations and flux profile. Q. J. R. Met. Soc. 109, 645–660.
Legg, B.J., Raupach, M.R., 1982. Markov chain simulation of particle dispersion in inhomogeneous flows: the mean drift velocity induced by a gradient in Eulerian velocity variance. Boundary-Layer Meteorol. 24, 3–13.
Ley, A.J., 1982. A random walk simulation of two-dimensional diffusion in the neutral boundary layer. Atmos. Environ. 16, 2799–2808.
Lin, C.C., Reid, W.H., 1962. In: Turbulent Flow. Handbuch der Physik, vol. 8/2. Springer, Berlin, pp. 438–523.
Ling, S.C., Kao, T.W., Asce, M., Saad, A., 1980. Microdroplets and transport of moisture from the ocean. J. Eng. Mech. Div. 6, 1327–1339.
Loth, E., 2001. An Eulerian turbulent diffusion model for particles and bubbles. Int. J. Multiphase Flow 27, 1051–1063.
Lopez de Bertodano, M., Lahey, R.T., Jones, O.C., 1994. Development of a k–ϵ model for bubbly two-phase flows. J. Fluids Eng. 116, 128–134.
Lyn, D.A., Stamou, A.I., Rodi, W., 1992. Density currents and shear-induced flocculation in sedimentation tanks. J. Hydraul. Eng., ASCE 118, 849–867.
MacInnes, J.M., Bracco, F.V., 1992. Stochastic particle dispersion modelling and the tracer-particle limit. Phys. Fluids A 4, 2809–2824.
Malin, M.R., Spalding, D.B., 1984. A two-fluid model of turbulence and its application to heated plane jets and wakes. PCH Phys.-Chem. Hydrodyn. 5, 339–362.
Mazumdar, D., Guthrie, I.L., 1995. The physical and mathematical modelling of gas-stirred ladle systems. ISIJ Int. 35, 1–20.
Meek, C.C., Jones, B.G., 1973. Studies of the behavior of heavy particles in a turbulent flow. J. Atmos. Sci. 30, 239–244.
Melville, W.K., 1996. The role of surface-wave breaking in air–sea interaction. Ann. Rev. Fluid Mech. 28, 279–321.
Meroney, R.N, Leitl, B.M, Rafailidis, S., Schatzmann, M., 1999. Wind-tunnel and numerical modeling of flow and dispersion about several building shapes. J. Wind Eng. Ind. Aerod. 81, 333–345.
Mestayer, P.G. et al., 1990. CLUSE simulations of vapor flux transformations by droplet evaporation. In: Mestayer, P.G., Monahan, E.C., Betham, P.A. (Eds.), Modelling the Fate and Influence of Marine Spray. Whitecap Report, 7. Mar. Sci. Inst., University of Conn, Groton, pp. 100–115.

Mestayer, P.G., Sini, J.F., Rey, C., Anquetin, S., Badri-Kusuma, S.M., Lakehal, D., 1993. Pollutant dispersion in the urban atmosphere: simulation of turbulent flows using a k–ϵ model. Ercoftac Bull. 16, 22–28.

Milelli, M., Smith, B.L., Lakehal, D., 2002a. Subgrid scale modelling in LES of turbulent bubbly flows. In: Proceedings of the TSFP-2, June 27–29, 2001, KTH Stockholm, Sweden. Journal of Turbulence (to appear).

Milelli, M., Smith, B.L., Lakehal, D., 2002b. Large-eddy simulation of turbulent shear flows laden with bubbles. In: Geurts, B.J, Friedrich, O., Métais, O. (Eds.), Direct and large-eddy simulation, 2001. ERCOFTAC series, vol. 8. IV. Kluwer Academic Publishers, pp. 461–470.

Moraga, F., Larreteguy, A.E., Drew, A., Lahey, R.T., 2001. Assessment of turbulent dispersion models for bubbly flows. In: Proceedings of the 4th conference. Multiphase Flow, New Orleans, May 27–June 1.

Mostafa, A.A., Mongia, H.C., 1987. On the modeling of turbulent evaporating sprays: Eulerian versus Lagrangian approach. Int. J. Heat Mass Transfer 12, 2585–2593.

Mosyak, A., Hetsroni, G., 1999. Direct numerical simulation of particle–turbulence interaction. Int. J. Multiphase Flows 25, 187–200.

Moussiopoulos, N., Theodoridis, G., Assimakopoulos, V., 1998. The influence of fast chemistry on the composition of NO_x in the emission input to atmospheric dispersion models. In: Borrell, P.M., Borrell, P. (Eds.), Proceedings of the EUROTRAC-2 Symposium on Transport and Chemical Transformation in the Troposphere, 1998, vol. 2. WIT Press/Computational Mechanics Publications, Southampton, pp. 777–781.

Murakami, S., 1997. Current status and future trends in computational wind engineering. J. Wind Eng. Ind. Aerod. 67/68, 3–34.

Nasstrom, J.S., Ermak, D.L., 1999. A homogeneous Langevin equation model, Part I: Simulation of particle trajectories in turbulence with a skewed velocity distribution. Boundary-Layer Meteorol. 92, 343–369.

Okong'o, N., Bellan, J., 2000. A priori subgrid analysis of temporal mixing layers with evaporating droplets. Phys. Fluids 12, 1573–1591.

Parker, D.S., Kinnear, D.J., Wahlberg, E.J., 2001. Review of Folklore in design and operation of secondary clarifiers. J. Environ. Eng. 127, 476–484.

Patton, E.G., Shaw, R.H., Judd, M.J., Raupach, M.R., 1998. Large-eddy simulation of windbreak flow. Boundary-Layer Meteorol. 87, 275–306.

Pope, S.B., 1987. Consistency conditions for random-walk models of turbulent dispersion. Phys. Fluids 30, 2374–2379.

Pope, S.B., 1994. Lagrangian PDF methods for turbulent flows. Annu. Rev. Fluid Mech. 26, 23–63.

Pozorski, J., Minier, J.P., 1998. On the Lagrangian turbulent dispersion models based on the Langevin equation. Int. J. Multiphase Flow 24, 913–945.

Pruppacher, H.R., Klett, J.D., 1978. Microphysics of Clouds and Precipitation. Reidel, Dordrecht.

Rafailidis, S., 2000. Near-field geometry effects on urban street canyon measurements for model validation. Int. J. Environ. Pollut. 14, 538–546.

Reid, J.D., 1979. Markov chain simulations of vertical dispersion in the neutral surface layer for surface and elevated releases. Boundary-Layer Meterol. 16, 3–22.

Rodi, W., 1987. Examples of calculation for flow and mixing in stratified fluids. J. Geophys. Res. 92, 5305–5328.

Rodi, W., Ferziger, J., Breuer, M., Pourquier, M., 1997. Status of large eddy simulation. Results of a Workshop. ASME J. Fluids Eng. 119, 248–262.

Sankaran, R., Paterson, D.A., 1997. Computation of rain falling on a tall rectangular building. J. Wind Eng. Ind. Aerod. 72, 127–136.

Sawford, B.L., Guest, F.M., 1991. Lagrangian statistical simulation of the turbulent motion of heavy particles. Boundary-Layer Meterol. 54,, 147–166.

Sawford, B.L., Yeung, P.K., 2001. Lagrangian statistics in uniform shear flow: direct numerical simulation and Lagrangian stochastic models. Phys. Fluids 13, 2627–2634.

Shabbir, A., Taulbee, D.B., 1990. Evaluation of turbulence models for predicting buoyant flows. J. Heat Transfer 112, 945–951.

Sheng, Y.Y., Irons, G.A., 1993. Measurement and modeling of turbulence in the gas/liquid two-phase zone during gas injection. Metall. Trans. B 24B, 695–705.

Snyder, W.H., Lumley, J.L., 1971. Some measurements of particle velocity autocorrelation functions in a turbulent flow. J. Fluid Mech. 48, 41–71.

Shirolkar, J.S., Coimbra, C.F.M., Queiroz McQuay, M., 1996. Fundamental aspects of modeling turbulent particle dispersion in dilute flows. Prog. Energy Combust. Sci. 22, 363–399.
Simonin, O., Viollet, P.L., 1988. On the computation of turbulent two-phase flows in the Eulerian formulation. In: EUROMECH 234, Toulouse, France.
Sini, J.F., Anquetin, S., Mestayer, P.G., 1996. Pollutant dispersion and thermal effects in urban street canyons. Atmos. Environ. 30, 2659–2677.
Smith, B.L., 1998. On the modelling of a bubble plume in a liquid pool. Appl. Math. Modelling 22, 773–797.
Smith, B.L., Milelli, M., 1998. An investigation of confined bubble plumes. In: Paper 641, 3rd International Conference on Multi-Phase Flow ICMF'98, Lyon.
Smith, S.D., Fairall, C.W., Geernaert, G.L., Hasse, L., 1996. Air–sea fluxes: 25 years of progress. Boundary-Layer Meteorol. 78, 247–290.
Sorbjan, Z., Uliasz, M., 1999. Large-eddy simulation of air pollution dispersion in the nocturnal cloud-topped atmospheric boundary layer. Boundary-Layer Meteorol. 91, 145–157.
Squires, K.D., Eaton, J.K., 1990. Particle response and turbulence modification in isotropic turbulence. Phys. Fluids A 2, 1191–1203.
Stull, R.B., 1988. An Introduction to Boundary Layer Meteorology. Kluwer Academic Publishers, Norwell, MA.
Szalai, L., Krebs, P., Rodi, W., 1994. Simulation of flow in circular clarifiers with and without swirl. J. Hydraul. Eng., ASCE 120, 4–17.
Takàcs, I., Patry, G.G., Nolasco, D., 1991. A dynamic model of the clarification-thickening process. Water Res. 25, 1263–1271.
Theodoridis, G., Moussiopoulos, N., 2000. Influence of building density and roof shape on the wind and dispersion characteristics in an urban area: a numerical study. Environ. Monitor. Assess. 65, 407–415.
Thomson, R., 1971. Numerical calculation of turbulent diffusion. Q. J. R. Met. Soc. 97, 93–98.
Thomson, D.J., 1987. Criteria for the selection of stochastic models of particle trajectories in turbulent flows. J. Fluid Mech. 180, 529–556.
van Kampen, N.G., 1992. Stochastic Processes in Physics and Chemistry. North-Holland, New York, p. 465.
van Marle, C., Kranenburg, C., 1994. Effects of gravity currents in circular secondary clarifiers. J. Environ. Eng., ASCE 120, 943–960.
Vitasovic, Z., Zhou, S., McCorquodale, J.A., Lingren, K., 1997. Secondary clarifier analysis using data from the Clarifier Research Technical Committee protocol. Water Environ. Res. 69, 999–1007.
Wang, M.C., Uhlenbeck, G.E., 1945. On the theory of Brownian motion II. Rev. Mod. Phys. 17, 323–341.
Wang, Q., Squires, K., 1996. Large eddy simulation of particle-laden turbulent channel flow. Phys. Fluids 8, 1207–1223.
Wells, M.R., Stock, D.E., 1983. The effect of crossing trajectories on the dispersion of particles in a turbulent flow. J. Fluid Mech. 136, 31–62.
Wilson, J.D., 2000. Trajectory models for heavy particles in atmospheric turbulence: comparison with observations. J. Appl. Meteorol. 39, 1894–1912.
Wise, A.F.E., 1965. Air flow round buildings. In: Proceedings of the Urban Planning Symposium, London, UK, 8 January 1965, pp. 71–91.
Yeh, F., Lei, U., 1991. On the motion of small particles in a homogeneous isotropic turbulent flow. Phys. Fluids A 3, 2571–2585.
Zhou, S., McCorquodale, J.A., Vitasovic, Z., 1992. Influences of density on circular clarifiers with baffles. J. Environ. Eng., ASCE 118, 829–847.
Zhou, Q., Leschziner, M.A., 1991. A time-correlated stochastic model for particle dispersion in anisotropic turbulence. In: Proceedings of the 8th Turbulent Shear Flow Symposium, Munich.
Zhou, S., McCorquodale, J.A., 1992. Modelling of rectangular settling tanks. J. Environ. Eng., ASCE 118, 1391–1405.